Bulletin of Earthquake Engineering (2025) 23:1759–1794
https://doi.org/10.1007/s10518-024-02025-5

ORIGINAL ARTICLE

Characterisation of the rigid diaphragm conditions for cross laminated timber floors

Giuseppe D'Arenzo[1] · Pietro Rigo[2,3] · Valentino Nicolussi[2,3] · Luca Pozza[2] · Daniele Casagrande[4]

Received: 18 April 2024 / Accepted: 24 September 2024 / Published online: 21 November 2024

Abstract
This paper presents a comprehensive numerical study aimed at defining the conditions for which Cross-Laminated Timber (CLT) floor diaphragms of platform-type CLT buildings can be assumed rigid in linear seismic analyses. Numerical analyses are conducted on a regular CLT archetype within a framework of parametric analyses, in which different geometrical and mechanical parameters including the stiffness of the floor panel-to-panel connections, the stiffness of the floor-to-wall connections, the floor span, the distance between two consecutive shear-walls, the lateral stiffness of the shear-walls, and the number of storeys are varied. The conditions to ensure a rigid diaphragm behaviour are derived by calculating the discrepancies in terms of floor displacements, distribution of lateral forces in the shear-walls, and fundamental vibration period of the structure, between numerical models where the floor is modelled with its actual deformability and as rigid. The discrepancies are compared with threshold values given in Eurocode 8 and used to derive the conditions for which CLT floor diaphragms can be assumed rigid. The study reveals that the behaviour of the floor tends toward the rigid diaphragm condition by increasing the stiffness of the floor panel-to-panel connections and the number of storeys, and by decreasing the stiffness of the floor-to-wall connections, the ratio between the distance between two consecutive shear-walls and the floor span, and the stiffness of the shear-walls. Specific threshold values ensuring a rigid diaphragm behaviour are determined for the properties of the system, delivering the geometrical and mechanical conditions for rigid CLT floor diaphragms.

Keywords CLT · Floors · Rigid diaphragm · Shear walls · Numerical analyses · Linear seismic analyses

1 Introduction

Floor diaphragms play a major role in the response of seismic force resisting systems (SFRS), transferring the inertia forces to the vertical structural elements and ensuring that the whole structural system responds as a single entity when subjected to seismic actions.

Extended author information available on the last page of the article

For this purpose, floor diaphragms are designed with an adequate in-plane stiffness and resistance and effective connections are adopted between the floors and the vertical elements of the SFRS.

A large in-plane stiffness of floor diaphragms is essential to limit the effects due to the in-plane deformations of floor elements on the distribution of the inertia forces on the vertical elements of the SFRS and to ensure the in-plane regularity in the seismic response of the whole structure. When a floor diaphragm has an in-plane stiffness adequately larger than that of the vertical elements, the seismic forces are distributed to the vertical elements proportionally to their stiffness and not to their tributary area.

Significant simplifications can also be adopted in the structural analysis and modelling of buildings when floor diaphragms can be regarded as rigid in their planes. The masses and the moments of inertia of each floor can be lumped at the centre of gravity of the floor and a diaphragm constraint can be adopted to connect a "master" joint, representing the centre of gravity, to all other "slaved" joints of such floor. The constrained joints move together as a planar diaphragm without affecting any out-of-plane deformation. A substantial reduction of the number of degrees of freedom and a consequent reduction of the computational effort is hence obtained when diaphragm constraints are adopted.

The rigid diaphragm conditions reported in international design codes and guidelines are typically based on the determination of the in-plane lateral displacements of the floors. The European code for seismic design of structures, the Eurocode 8 (EC8) (EN1998-1), assumes that a floor diaphragm can be taken as rigid if the lateral displacements of the floor obtained from considering its actual in-plane flexibility do not exceed by more than 10% those resulting from the rigid diaphragm assumption. According to ASCE 41-17 (ASCE 2017), a floor diaphragm is conversely rigid when the lateral displacements of the floor are less than or equal to half of the average drift of the inter-storey below the floor considered. Less stringent conditions are applied by the American International Building Code (IBC) (International Code Council (ICC) 2018), where a floor diaphragm can be assumed to be rigid for the purpose of distribution of shear forces and torsional moments when the lateral displacements of the floor are less than or equal to two times the average drift of the inter-storey below the floor considered. The verification of the rigid diaphragm assumptions can hence be performed only through the calculation of the lateral displacements of floor diaphragms where their actual in-plane deformation is considered. As a result, a substantial simplification in the structural analysis cannot be achieved if the actual in-plane flexibility of floor diaphragms is implemented in the models of analysis.

As an alternative to rigorous conditions based on determination of the in-plane lateral displacements of the floors through numerical models, some international codes (e.g. EC8) report prescriptive provisions under which floor diaphragms can be regarded as rigid. Structural details (e.g. minimum thickness of the topping layer in reinforced concrete slabs), geometrical limitations (e.g. maximum span between vertical supports) and design rules apply when floor diaphragms are taken as rigid.

Regarding timber structures, Eurocode 8 provides prescriptive provisions and detailing rules for light-frame floors assembled with wood-based panels connected to timber beams by mechanical fasteners. For such floor type, the rigid floor diaphragm condition can be assumed to be satisfied when transverse blocking elements are placed between the timber beams ensuring the nailing of all sheathing edges, no change of span-direction of the beams over supports occurs, and openings do not significantly affect the in-plane stiffness of the

floor diaphragms. Conversely, neither prescriptive provisions nor design rules are currently reported for Cross-Laminated Timber (CLT) floor diaphragms. As a result, the verification of rigid diaphragm conditions for CLT floors can be performed only through numerical analyses where their actual in-plane stiffness is considered.

The absence of prescriptive rigid diaphragm conditions for CLT floors also in other international design codes and the review of the available literature, reported and discussed in the next sections, highlights the need to establish better understanding of the conditions under which CLT floors can be regarded as rigid. An in-depth investigation concerning which values of structural and geometrical parameters should be considered in the design process with the aim of assuming a rigid in-plane behaviour of CLT floors has not yet been undertaken.

This paper presents the results of a parametric analysis aimed at the definition of the in-plane rigid diaphragm conditions for CLT floor diaphragms. Through a comprehensive study of the available literature and extensive numerical analyses, the conditions that assure a rigid behaviour of CLT floor diaphragms in CLT platform-type buildings are identified and discussed. Linear structural analyses, which represent one of the primary analysis types used for the seismic design of buildings, are employed in the study.

The influence of the geometrical and mechanical parameters adopted in the design of CLT floor components (CLT panels and connections) on i) the distribution of elastic inertia forces among the vertical elements of the SFRS, ii) the relative in-plane deformation of CLT floor diaphragms and iii) the natural period of CLT platform-type buildings is analysed as well. Two case studies of two CLT platform-type buildings were also conducted to demonstrate the validity of the rigid diaphragm conditions obtained from the parametric analyses, as detailed in Appendix A.

2 State of the art

Several research studies have been conducted in the last decade to investigate the in-plane flexibility of CLT floor diaphragms. The studies have been carried out both at floor level on full-scale floor diaphragms and on connections used to connect the CLT floor panels one-to-another and to CLT walls underneath. A comprehensive state-of-the-art review on performance, analysis, and design of mass timber (e.g. CLT) diaphragms was presented by Popovski et al. (2023), summarizing the information available in the literature and in some international building codes.

2.1 Studies at floor level

Four cyclic tests on two 5.00×4.27 m full-scale CLT floor diaphragms were conducted by Kode et al. (2021) under two different floor layouts, namely simple-span and two-span continues panels, in a cantilever test configuration. The test results revealed a rigid behaviour of the CLT panels and the energy dissipation in the connections, highlighting the importance of tension chords in the transmission of internal forces. Similar outcomes were obtained from the two full-scale 7.32×7.32 m CLT diaphragms monotonically tested by Line et al. (2022). The experimental campaign was conducted by means of a single-span test configuration with the aim to verify design provisions on CLT diaphragms reported in ANSI/AWC 2021.

The failure mechanisms were observed in the panel-to-panel and panel-to-beam connections while neither significant deformations nor failure of the CLT panels occurred. The tests confirmed the adequacy of the design provision reported in the ANSI/AWC 2021.

Two different 7.30 × 2.40 m CLT diaphragms with different configurations were tested in Canada under a single-span test configuration by Popovski et al. (2023). Differently from the tests conducted by Kode et al. (2021) and Line et al. (2022), where multi-panel CLT floors were tested, both a multi-panel (i.e. 3-panel) and a single panel CLT floor configuration was analysed to investigate the role of panel-to-panel connections. The results confirmed the strong influence of the panel-to-panel connections on the diaphragm's behaviour as demonstrated by the reduction of stiffness (i.e. 43%) from the single- to the 3-panel floor configuration. With the primary goal of investigating the interactions between the CLT panels and connections, assessing the in-plane ductility of CLT floor diaphragms as well as compare the real performance of CLT diaphragms systems with that assumed in practice, Beairsto et al. (2022) conducted a comprehensive experimental campaign on twenty-eight full-scale 4.57 × 4.57 m CLT floor specimens composed of three panels by means of monotonic and cyclic tests. Different numbers of chord and panel-to-panel screw spacing as well as two different CLT panel wood species, Douglas fir–larch and spruce-pine-fir, were considered in the definition of the test matrix. The test results showed that the flexibility and ductility of CLT floor diaphragms is primarily influenced by the panel-to-panel connections.

Barbosa et al. (2018) investigated the behaviour of a 6.10 × 17.7 m CLT floor diaphragm by means of a shake-table test on a 2-storey timber building. Two different diaphragm CLT types were used: i) at the first floor, a CLT diaphragm composed of sixteen panels connected by means of spline joints, ii) at the roof level, a CLT-concrete composite diaphragm. Both CLT floors were designed to remain elastic during the simulated seismic events. Accelerations at different locations of the CLT floors were measured during the shake-table tests to evaluate the flexibility of the floor diaphragm. The results showed a non-uniform response of the first-floor diaphragm (i.e., the diaphragm cannot be regarded as rigid) whereas for the CLT-concrete composite diaphragm exhibited a more uniform acceleration pattern due to the increased stiffness provided by the concrete top. Valuable information on the in-plane behaviour of CLT floor diaphragm was also obtained from the cyclic test conducted by Popovski and Gavric (2016) on a two-storey full-scale platform-type CLT structure mock-up. In this case, the results showed negligible in-plane deformations of the floor diaphragms, which acted as rigid.

Loss and Frangi (2017) and Loss et al. (2018b) investigated an innovative steel-timber hybrid floor diaphragm with modular prefabricated composite elements by means of experimental tests and numerical analyses. The results of the experimental tests showed that the main deformations of the floor were localised at the beam-to-beam steel joints while the steel-CLT hybrid elements behaved elastically without failure.

Ashtari et al. (2014) analysed the in-plane behaviour of CLT floor diaphragm by means of Finite Element (FE) numerical models. A parametric analysis was conducted on a CLT diaphragm with the aim of investigating the geometrical and mechanical parameters on the in-plane stiffness of CLT floor diaphragms. The lateral load distribution on shear-walls supporting the analysed floor obtained from the FE analyses were compared to those determined by two theoretical distributions, namely the tributary area and stiffness method, adopted in the design procedure in case of flexible and rigid floor diaphragms, respectively. Moroder (2016) and Moroder et al. (2015) presented a comprehensive study on the influence of dia-

phragm stiffness on the dynamic behaviour of multi-storey timber buildings. The results showed that the in-plane behaviour of CLT floor diaphragms can be well described through an Equivalent Truss Model. Fakhrzarei et al. (2024) conducted a numerical parametric study on CLT diaphragm deflection, highlighting the critical role of panel-to-panel connection stiffness. It was found that panel thickness and connection stiffness impact deformation differently based on load orientation, with staggered panel layouts offering generally better load distribution and higher capacity.

A parametric numerical analysis was conducted by D'Arenzo et al. (2019) to investigate the in-plane flexibility of CLT floor diaphragms and major deformation contributions. Assuming that a CLT floor behaves like a deep beam, the diaphragm total deformation can be mainly split into shear and bending contributions as shown in Fig. 1. The deformation contribution to shear (Δ_s) is given by (1) the in-plane deformation of the panels (Δ_G), (2) the panel-to-panel connections acting parallel to the panel joints ($\Delta_{f\text{-}f}$) and (3) the floor-to-wall connections along the shear-walls parallel to floor span ($\Delta_{f\text{-}w}$). The bending contribution (Δ_b) is conversely given by: (4) in-plane bending stiffness of CLT panels, (5) the panel-to-panel connections acting perpendicular to the panel joints and (6) the floor-to-wall connections along the shear-walls perpendicular to the floor span. The results of this study showed that the in-plane flexibility of CLT floor diaphragms is primarily governed by the panel-to-panel connections, that CLT panels have a negligible influence on the floor in-plane flexibility, as well as that floor-to-wall connections along the shear-walls perpendicular to the floor span, act as a chord element.

2.2 Studies at connection level

The review of the available literature reveals that the in-plane behaviour of CLT floor-diaphragms is primarily governed by two types of connections: connections used to connect CLT panel one-to-another (i.e. floor panel-to-panel connections) and those adopted to connect the CLT floor panels to the walls below (i.e. floor-to-wall connection). In this subsection, a summary of the experimental campaigns conducted on such connections is reported with the aim of defining a reasonable range of stiffness values to be used in the parametric analysis presented in the current study and described in the next section.

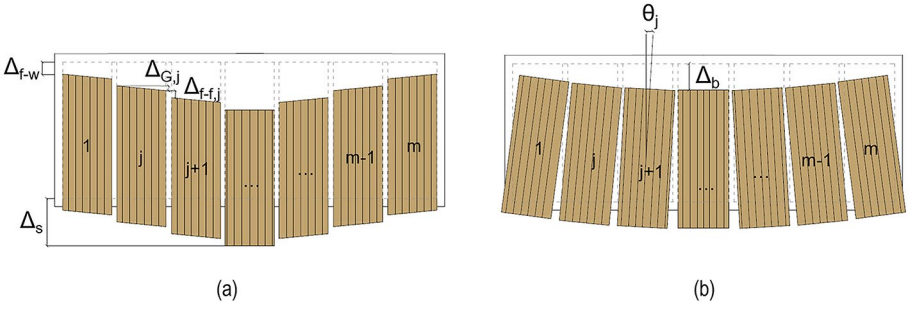

Fig. 1 CLT floor diaphragm in-plane deformation mechanism readapted from D'Arenzo et al. (2019): **a** shear deformation, **b** bending deformation

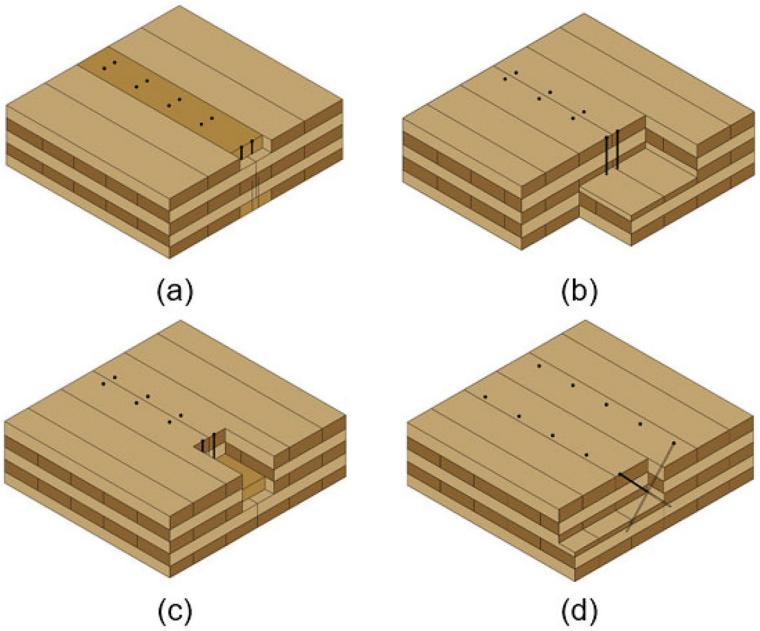

Fig. 2 Examples of floor panel-to-panel connections: **a** outer spline-, **b** lap-, **c** inner spline- and **d** butt-joints

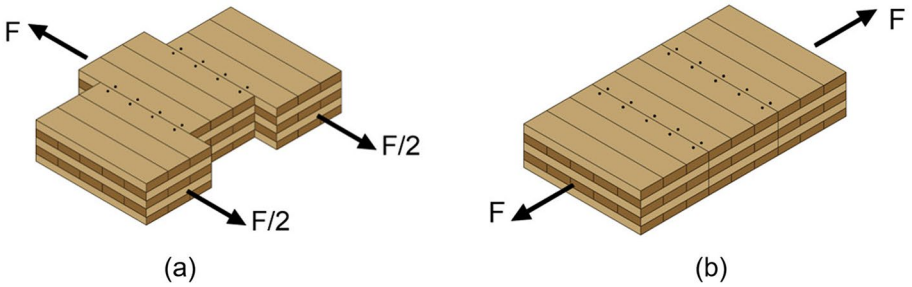

Fig. 3 Direction of the mechanical behaviour of the panel-to-panel joints considered in the study: **a** parallel to the joint, **b** perpendicular to the joint

2.2.1 Floor panel-to-panel connections

Four types of joints are typically used to connect CLT panels one-to-another, namely outer spline-, inner spline-, lap-, and butt-joints, see Fig. 2, where either nails, partially threaded screws (PTSs) or fully threaded screws (FTSs) may be adopted. The mechanical performance of such joints was investigated with reference to in-plane loads acting either parallel or perpendicular to the joint direction (Fig. 3).

Lap-joints with five different types of PTSs, namely 6×80 mm, 6×120 mm, 8×80 mm, 10×140 mm and 8×90 mm were tested by Flatscher (2017), Gavric et al. (2015), Hossain et al. (2019) and Yin et al. (2022) with loads acting parallel to the joint direction. In those tests,

a range of stiffness per fastener equal to 0.19 ÷ 1.27 kN/mm was determined. Lap-joints with 8 × 140 mm FTSs were also tested by Hossain et al. (2019) showing values of stiffness per fastener between 2.70 and 4.70 kN/mm. Spline joints with 8 × 80 mm PTSs were tested by Gavric et al. (2015) and Hossain et al. (2019) showing values of stiffness per fastener between 0.42 and 2.00 kN/mm.

For butt joints significant higher values of stiffness were found than those obtained for lap- and spline-joints. Loss et al. (2018a) investigated the mechanical performance of panel-to-panel connections in butt-joint configuration by using PTSs and FTSs arranged in different inclinations, with screw diameters between 10 and 12 mm and lengths between 140 and 200 mm. The results of this experimental study showed that the butt joint connections cover a wide range of stiffness per fastener, ranging from 1.05 to 5.00 kN/mm. The stiffness is largely influenced by the screw length as well as the insertion angle. Similar tests were conducted by Hossain et al. (2019) on butt-joints with 8 × 140 mm FTSs. Also in this case, different insertion angles were adopted, which brought to a wide range of stiffness per fastener, ranging from 0.40 to 7.50 kN/mm.

Limited information is available on the mechanical behaviour of panel-to-panel connections subjected to an action perpendicular the joint directions. Gavric et al. (2015) tested lap-joints, where 8 × 80 mm and 10 × 140 mm PTSs were used, and spline joints with 8 × 80 mm PTSs, obtaining values of stiffness per fastener between 0.83 and 1.25 kN/mm. Butt-joints with inclined 11 × 100 mm FTSs were tested by Xiong and Huynh (2018) determining a stiffness per fastener equal to 2.66 kN/mm.

2.2.2 Floor-to-wall connections

Screwed connections are typically adopted to connect CLT floor panels to wall panels below. PTSs can be inserted in the narrow face of the wall panel with a small out-of-plane inclination (i.e. 10°-15°), see Fig. 4 *a*, and are designed to transfer the floor-to-wall shear load primarily acting in shear. Conversely, FTSs are usually 45° driven in the narrow face of the wall panel, transferring the floor-to-wall shear load primarily acting axially in tension or compression, see Fig. 4 *b*.

Flatscher (2017) and Gavric et al. (2015) tested three floor-to-wall connections with three different types of PTSs, namely 8 × 280 mm, 10 × 180 mm and 10 × 260 mm. A stiffness per fastener equal to 0.46 kN/mm, 1.49 and 1.45 kN/mm was found, respectively.

Brown et al. (2021) investigated the mechanical performance of perpendicularly arranged wall-to-wall connections where 8 mm FTSs with lengths between 200 and 400 mm and with different inclinations were used. Despite such tests were conducted on connections between two perpendicular walls, the results can be extended to the case of floor-to-wall connections. The results showed a range of stiffness per fastener, ranging from 0.80 to 11.25 kN/mm, largely depending on the screw length and inclination. Floor-to-wall connections with 45° inclined 7 × 140 mm FTSs were tested by Xiong and Huynh (2018), where a stiffness per fastener equal to 0.95 kN/mm was obtained.

A summary of the values of stiffness per fastener obtained from the tests available in literature on panel-to-panel and floor-to-wall connections are reported in Table 1. The table also reports the inclination of the screws according to angles shown in Fig. 5. It can be observed that the range of stiffness are relatively wide, due to the significant influence of the properties reported in Table 1.

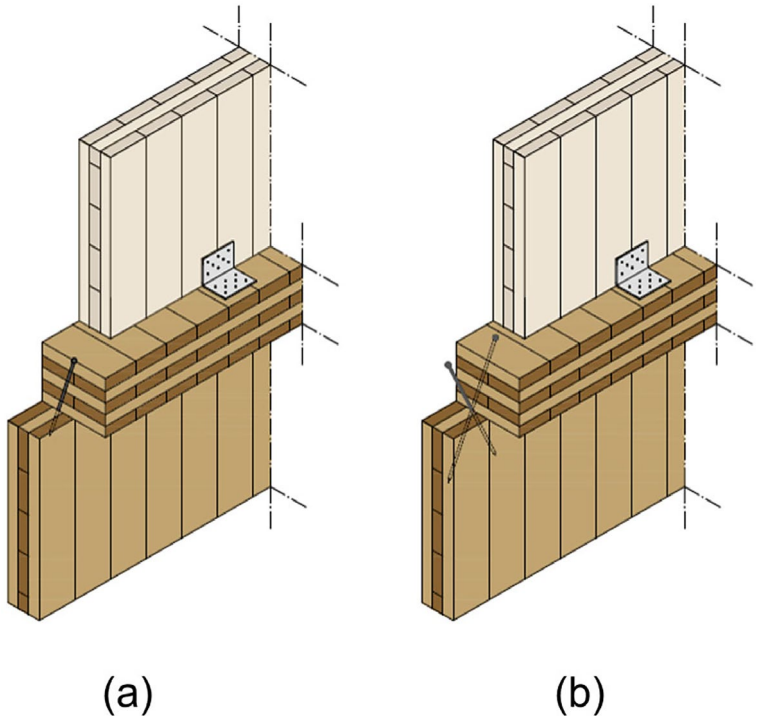

Fig. 4 Examples of floor-to-wall connections with **a** PTSs and **b** FTSs

3 Parametric analysis: methodology

A parametric analysis was conducted to define the in-plane rigid diaphragm conditions by means of numerical analyses. The analyses were performed on a regular CLT archetype with the aim of studying the influence of geometrical and mechanical parameters adopted in the design of CLT floor components (CLT panels and connections) on: i) the distribution of elastic inertia forces among the shear-walls of the SFRS, ii) the relative in-plane deformation between the CLT floor diaphragms and the shear-walls and iii) the natural vibration period of the archetype.

3.1 Description of the archetype

A symmetric multi-storey CLT platform archetype with a rectangular plan of dimensions $B \times L$ is selected for the parametric analysis. At each storey, the archetype is characterized by three longitudinal and two transversal single-panel CLT shear-walls with height h, see Fig. 6.

The two transversal shear-walls (W1T and W2T) and two of the longitudinal shear-walls (W1L and W3L) are placed on the perimeter of the archetype plan, while the longitudinal wall W2L is aligned along the archetype longitudinal symmetry axis. The length of each transversal and longitudinal wall is equal to B and L, respectively. The distance between the central shear-wall W2L and each of the two outer longitudinal wall (W1L and W3L)

Table 1 Summary of the values of stiffness per fastener obtained from the tests available in literature on floor panel-to-panel and floor-to-wall connections

Panel-to-panel connections //	Screw types	Diameter and length of screws	Inclination of screw (α_1, α_2)	References	Stiffness per fastener
Lap joint	PTS, FTS	6 × 80 mm; 6 × 120 mm; 8 × 80 mm; 8 × 90 mm; 8 × 140 mm;	(0°,0°); (90°,45°); (0°,0°); (0°,0°); (0°,0°) & (90°,45°);	Flatscher (2017), Gavric et al. (2015), Hossain et al. (2019) and Yin et al. (2022)	0.19 ÷ 4.70 kN/mm
Spline joint	PTS	8 × 80 mm	(0°,0°);	Gavric et al. (2015) and Hossain et al. (2019)	0.42 ÷ 2.00 kN/mm
Butt joint	PTS, FTS	10 ÷ 12 × 140 ÷ 200 mm; 8 × 140 mm; 8 × 180 mm;	(90°,45°) & (90°,60°) & (60°,45°) & (60°,60°); (90°,45°); (67°,45°);	Loss et al. (2018a), Hossain et al. (2019)	0.40 ÷ 7.50 kN/mm
		Total range			0.19 ÷ 7.50 kN/mm
Panel-to-panel connections ⊥	Screw types	Diameter and length of screws	Inclination of screw (α_1, α_2)	References	Stiffness per fastener
Lap joint	PTS	8 × 80 mm; 10 × 140 mm;	(0°,0°); (0°,0°);	Gavric et al. (2015)	0.83 ÷ 1.25 kN/mm
Spline joint	PTS	8 × 80 mm;	(0°,0°);	Gavric et al. (2015)	0.94 kN/mm
Butt joint	FTS	11 × 100 mm;	(90°,45°);	Xiong and Huynh (2018)	2.66 kN/mm
		Totale range			0.83 ÷ 2.66 kN/mm
Floor-to-wall connections	Screw	Diameter and length	Inclination of screw (α_1, α_2)	References	Stiffness per fastener
With PTSs	PTS	8 × 280 mm; 10 × 180 mm; 10 × 260 mm;	(0°,0°); (0°,0°); (0°,0°);	Flatscher (2017), Gavric et al. (2015),	0.46 ÷ 1.49 kN/mm
With FTSs	FTS	8 × 200 ÷ 400 mm; 7 × 140°mm;	(0°,0°) & (15°,30°); (90°,45°);	Brown et al. (2021), Xiong and Huynh (2018)	0.80 ÷ 11.25 kN/mm
		Total range			0.46 ÷ 11.25 kN/mm

is equal to *i*. The floors are made with CLT panels aligned along the longitudinal direction and simply supported by the two transversal walls. The length of each floor panel is equal to the longitudinal dimension *L* of the archetype, whereas *b* is the width of each floor panel.

Five different configurations of archetypes in terms of number of storeys *N*, namely one to five, were considered with a constant inter-storey height *h* equal to 3.18 m, as shown in Fig. 7. For each configuration three different values of the distance *i* between the central shear-wall W2L and each of the two outer longitudinal walls were analysed, namely equal to 3, 5 and 7 m, resulting in a total transversal length *B* of the archetypes equal to 6, 10 and 14 m, respectively. The total longitudinal length *L* of the archetypes was conversely taken

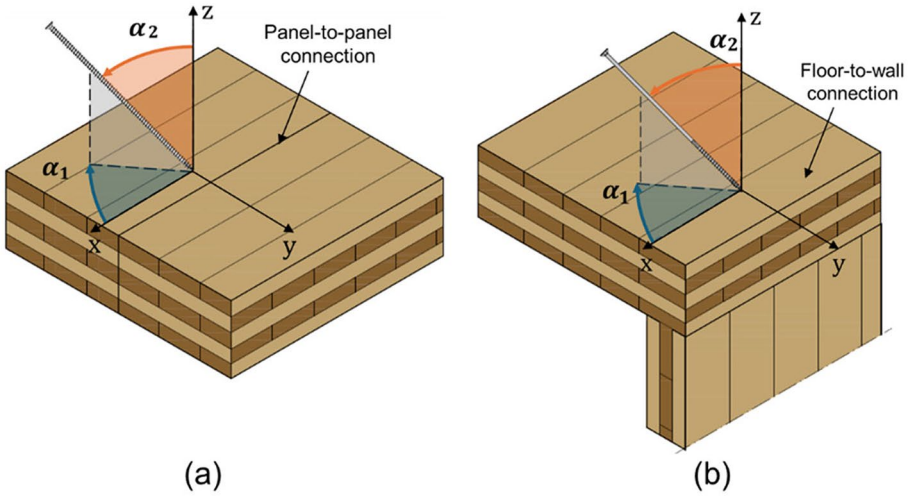

Fig. 5 Reference system used to measure the inclination of the screws

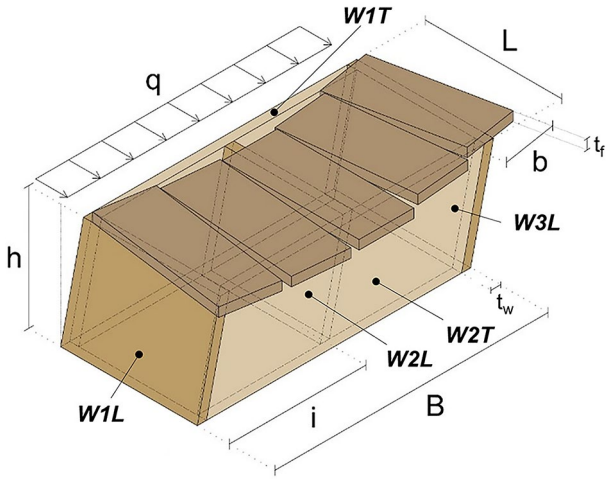

Fig. 6 CLT platform archetype considered in the parametric analysis

equal to 5 m for all configurations. A uniformly distributed lateral load q of 2.50 kN/m, applied along the transversal direction, is applied on the floor at each storey, see Table 2 and Fig. 7. The magnitude of the load was calculated by considering the seismic weight of a typical residential CLT building and an earthquake design spectrum with a peak ground acceleration of 0.25 g. Moreover, a distribution of loads along the building height proportional to the masses, according to Eurocode 8 provisions, was adopted. It should be noted that, since linear analyses are conducted, the results are influenced only by the distribution of the load along the building height and not by its magnitude.

In order to replicate realistic choices, the thickness and layout of the CLT panels for the shear-walls varied along the height of the archetype, where lower storey panels were assigned thicker panels. Four different types of the 5-ply CLT panels with orientation of

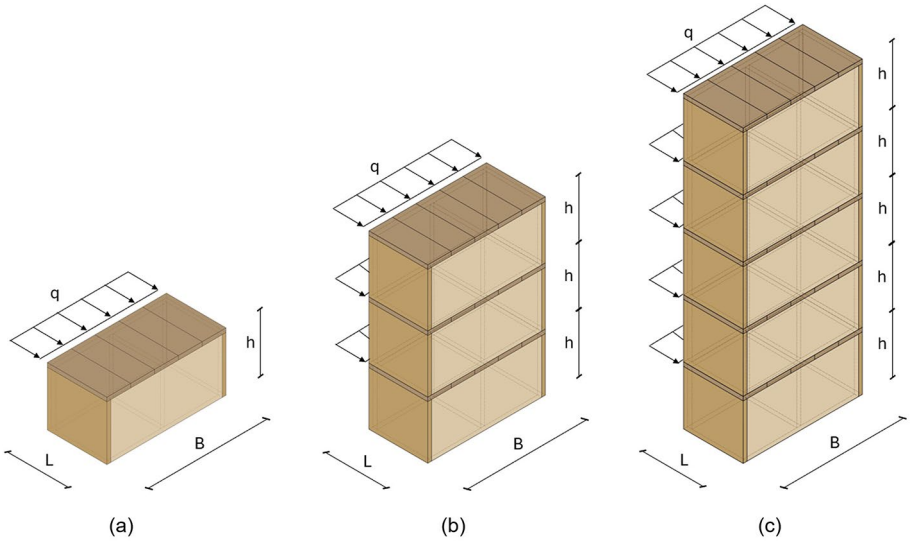

Fig. 7 CLT platform archetype configurations of number of storeys N: **a** single-storey, **b** three-storey, **c** five-storey

Table 2 Summary of the geometrical and mechanical parameters of the multi-storey CLT platform archetype considered in the parametric analysis

Parameter	Symbol	Values
Archetype longitudinal dimension; i.e. length of longitudinal walls	L [m]	5
Archetype transversal dimension; i.e. length of transversal walls	B [m]	6;10; 14
Height of CLT wall panel	H [m]	3
Inter-storey height	h [m]	3.18
Number of storeys	N [-]	1;2;3;4;5
Floor panel length	L [m]	5
Floor panel width	b [m]	2
Floor panel thickness	t_f [mm]	179
Wall panel thickness	t_w [mm]	100; 124; 137; 158
Horizontal load at each storey	q [kN/m]	2.50

outer lamination along the vertical direction were selected, namely 100 (17-17-32-17-17) mm, 124 (17-17-32-17-17) mm, 137 (33–19-33–19-33) mm and 158 (40-19-40-19-40) mm (the bold notation was used to mark the layers parallel to the vertical direction). According to (ETA-Denmark 2018), an elastic modulus parallel to the grain $E_0 = 11.5$ GPa and a shear modulus $G_0 = 0.69$ GPa are assumed for the CLT laminations. The width of lamination was assumed to be equal to 200 mm. 5-ply 179 (30-40-33-40-33) mm thick CLT panels were selected for the floor of all storeys. The width and length of the floor panels are equal to 2 m and 5 m, respectively. As for the wall panels, an elastic modulus parallel to the grain $E_0 = 11.5$ GPa and a shear modulus $G_0 = 0.69$ GPa are considered for the CLT laminations.

The angle brackets used in this study are of type AE116 (ETA-Denmark 2016) and they were supposed to be connected to the wall panel by means of 25 annular ring nails 4 × 60 mm. The types of hold-down device selected are WHT 340, WHT440 and WHT620 (ETA-Denmark 2015) connected to the wall panel by means of 20, 35 and 55 4.0 × 60 mm annular ring nails. A bi-directional behaviour of the angle-brackets is assumed in the analyses with a value of stiffness along the tensile-vertical and shear-horizontal direction equal to 5.98 kN/mm and 2.89 kN/mm, respectively. The hold-downs are conversely considered to be effective along the tensile-vertical direction with a value of stiffness equal to 5.70, 6.61, 13.25 kN/mm for WHT 340, WHT440 and WHT620, respectively.

The number and types of angle-brackets and hold-down selected for all shear-walls at each storey was varied along the height of the building due to the cumulative lateral shear force and overturning moment acting on the shear-walls, as reported in Table 3.

In order to take into account the influence on the lateral stiffness of shear-walls on the plane rigid diaphragm conditions of CLT floors, three different configurations of archetypes in terms of shear-wall stiffness were considered (*S1*, *S3* and *S5*). All three configurations of archetypes were characterized by the same type and number of the angle-brackets and hold-down reported in Table 3; however, the stiffness of angle-brackets and hold-down used in configuration *S1* were increased for configurations *S3* and *S5* in the analyses by a factor of 3 and 5, respectively, with the aim of simulating stiffer connections. The value of stiffness of the longitudinal shear-walls for configurations *S1*, *S3* and *S5* were calculated according to the analytical procedure reported in Sect. 3.3 and are equal to 10,382 kN/m, 31,163 kN/m and 51,939 kN/m, respectively.

Different types of screwed panel-to-panel connections and floor-to-wall connections as well as fastener spacing were selected in order to investigate the influence of such types of connections on the rigid diaphragm conditions of CLT floors. Similarly to the strategy adopted for the shear-walls, three different configurations were selected for both floor panel-to-panel connections and floor-to-wall connections, corresponding to three different values namely low (L), medium (M) and high (H), of stiffness per unit length.

The experimental studies on screwed floor panel-to-panel connections reported in Sect. 2.2.1 reveal that the majority of the values of stiffness per fastener are in the range of 0.5–5 kN/mm (outer values are neglected in this case), both in direction parallel and perpendicular to the joint direction. Considering a realistic spacing between 200 and 250 mm, a realistic range of stiffness per unit length of screwed panel-to-panel connections is 2– 20 kN/mm^2. As a result, the stiffness of floor panel-to-panel connections per unit length $K_{f\text{-}f}$ were taken equal to 2, 8 and 20 kN/mm^2 for the low, medium and high floor panel-to-panel stiffness configuration, respectively.

Table 3 Distribution of CLT panel and connections along the height of the buildings considered in the parametric analysis

Storey	1-Storey archetype			3-Storey archetype			5-Storey archetype		
	t_w [mm]	HD No.-type	AB No	t_w [mm]	HD No.-type	AB No	t_w [mm]	HD No.-type	AB No
5th							100	1 WHT340	4
4th							100	1 WHT540	6
3rd				100	1 WHT340	4	124	1 WHT620	8
2nd				100	1 WHT540	6	137	2 WHT620	10
1st	100	1 WHT340	4	124	1 WHT620	8	158	3 WHT620	12

Analogously, the values of stiffness per fastener obtained from the experimental tests of the floor-to-wall connections reported in Sect. 2.2.2 cover a range approximately between 0.5 to 12 kN/mm. Considering a realistic spacing between 150 and 250 mm, a realistic range of stiffness per unit length of screwed floor-to-wall connections is 3–45 kN/mm^2. The stiffness of floor-to-wall connections per unit length $K_{f\text{-}w}$ were taken equal to 3, 15 and 45 kN/mm^2 for the low, medium and high floor-to-wall stiffness configuration, respectively.

A total of five different configurations of archetypes in terms of number of storeys with three different values of total transversal length, three different values of shear-wall stiffness, three different values of floor panel-to-panel floor stiffness and three different values of floor-to-wall stiffness were analysed, yielding a total of 405 case studies.

3.2 Finite element numerical model

The numerical analyses were conducted by means of the commercially available finite element (FE) software package SAP2000 [20]. Four-node quadrilateral homogenous shell elements were adopted to model both wall and floor CLT panels. A 200 mm meshing size was selected based on a mesh analysis, in order to achieve a reasonable balance between accuracy and computation effort. Effective values of the modulus of elasticity along the vertical, $E_{eff,v}$, and horizontal, $E_{eff,h}$, as well as of the in-plane shear modulus, G_{eff} were determined as expressed by Eqs. (1) to (3) to take into account the orientation and lay-up of the CLT panels according to Bogensperger et al. (2010) and Brandner et al. (2017).

$$E_{\mathrm{eff,v}} = \frac{E_0 t_v + E_{90} t_h}{t_{CLT}} \tag{1}$$

$$E_{\mathrm{eff,h}} = \frac{E_0 t_h + E_{90} t_v}{t_{CLT}} \tag{2}$$

$$G_{\mathrm{eff}} = \frac{G_0}{1 + 6\alpha_T \left(\frac{t_{mean}}{w}\right)^2} \tag{3}$$

In Eqs. (1) to (3), E_0 and E_{90} are the moduli of elasticity in the direction parallel and perpendicular to the lamination, t_v and t_h represent the total thickness of the vertical and horizontal lamination, t_{CLT} is the total thickness of the CLT panel, G_0 is the in-plane shear modulus of the lamination, w is the width of the lamination, t_{mean}, defined in Eq. (4), represents the mean thickness of the lamination, and α_T can be calculated by using Eq. (5).

$$t_{mean} = \frac{t_{CLT}}{n_{lay}} \tag{4}$$

$$\alpha_T = p\left(\frac{t_{mean}}{w}\right)^{-0.79} \tag{5}$$

In Eq. (4) and (5), n_{lay} is the number of the layers and p is a parameter equal to 0.535, for three-layered CLT panels, and 0.425, for five-layered CLT panels.

The hold-down and the angle brackets at the first and upper storeys were modelled by means of one-joint and two-joint multi-linear link elements, respectively, see Fig. 8. The mechanical behaviour of hold-downs and angle brackets in the tensile-vertical direction was represented by a bi-linear curve, characterized by the corresponding tensile stiffness k_h and $k_{a,z}$ when subject to a tensile actions and a rigid behaviour when subjected to compression. The behaviour of angle-brackets along the shear-horizontal direction was assumed to be linear with a value of stiffness $k_{a,x}$. Vertical gap elements were located along the entire base of the wall panels to simulate the contact with either the floor below (for the uppers storeys) or the ground (for the first storeys). To prevent the horizontal displacement in the out-of-plane direction of walls, rigid translation restrains were added at the bottom of each wall at the ground floor.

Floor-to-wall connections were modelled as two-joint vertical link elements equally spaced with a linear elastic behaviour acting along both the longitudinal and transversal direction. The value of stiffness of each link was determined as the product of the selected floor-to-wall connection stiffness per unit length multiplied by the mesh size.

Two-joint horizontal link elements were adopted to model the floor panel-to-panel connections. A linear elastic behaviour was assumed in the direction parallel to the joint whereas a bilinear elastic behaviour was adopted in the transversal direction to simulate both the separation and the contact of the panel one-to-another. The same values of stiffness, determined as the product of the selected floor panel-to-panel connection stiffness per unit length and the mesh size, was used for the longitudinal direction and the transversal direction under tensile loads. A rigid behaviour was assumed to simulate the contact of the panels in the transversal direction.

The effect of connections between the longitudinal and perpendicular walls (D'Arenzo et al. (2024)) and the contribution of vertical load on wall kinematic mechanism was ignored in the model. The comprehensiveness of the study will be achieved by introducing these two effects in ongoing and future research effort.

For the numerical models representing the cases with rigid diaphragms, rigid diaphragm constraints were applied to all the joints of the same floor level, see Fig. 9. The constrained joints of a certain floor were hence restrained to move together as a planar diaphragm that is

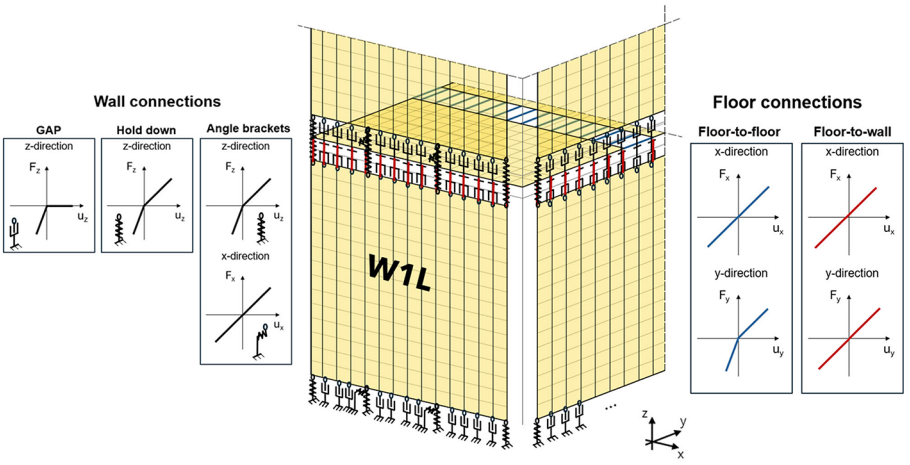

Fig. 8 Numerical model of CLT archetype with non-rigid floors

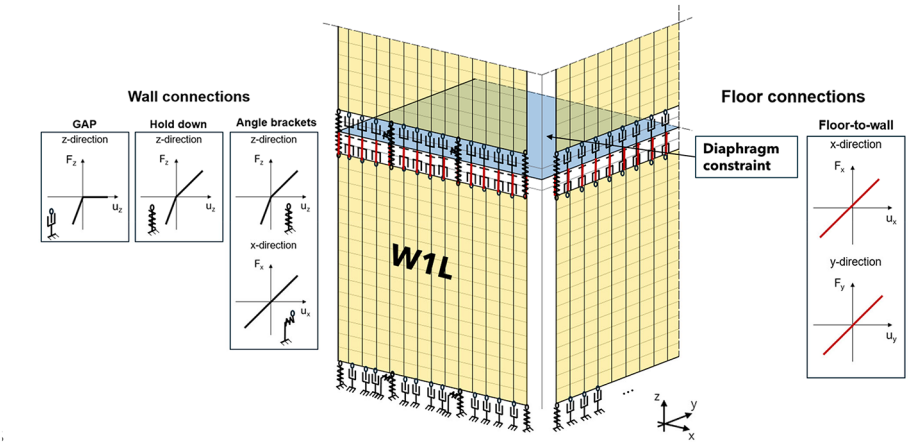

Fig. 9 Numerical model of CLT archetype with rigid floor diaphragm constraint

rigid against membrane deformations. Non-linear elastic static analyses were conducted in order to take the non-linearity due to gap, hold-down, and angle bracket elements.

The adopted numerical modelling strategy is consistent with those presented in the literature. While the modelling approach for the walls follows established methods (see, for instance, Ruggeri et al. (2023) and Casagrande et al. (2021)), the modelling strategy for the floor has been further validated experimentally, as detailed in Appendix B.

3.3 Method of analysis

For each CLT archetype considered in the parametric study, the structural analysis was carried out first on the model with the actual deformation (i.e. non-rigid floor model (Fig. 8)) of the floor diaphragm and then on the model with rigid diaphragm (i.e. where rigid diaphragm constraints were applied (Fig. 9)), considering different parameters related to the in-plane behaviour of the floor.

According to the definition of rigid diaphragm condition given in Eurocode 8, the maximum floor displacements of the non-rigid floor model can be obtained from those obtained from the models with rigid diaphragm as expressed by Eq. (6), where the parameter α_δ, represents the increase of displacement when the floor is modelled with its actual deformation and the subscripts *NR* and *R* refer to "Non-Rigid" and "Rigid" floor conditions, respectively. The rigid floor diaphragm condition reported in Eurocode 8 is in fact based on the limit value of the parameter α_δ, equal to 0.1 (i.e. 10%).

$$\delta_{NR} = (1 + \alpha_\delta)\delta_R \tag{6}$$

Furthermore, the comparison between the non-rigid floor and rigid floor models was conducted in terms of two additional parameters, namely the shear force V acting on the central shear-wall W2L and the natural vibration period T of the archetype. The discrepancies between the two models for both parameters were calculated according to Eq. (7) and Eq. (8). It should be noted that as the parameters α_δ, ε_V, and ε_T decrease, the behaviour of the floor tends towards the rigid condition.

$$\varepsilon_V = \frac{V_{NR} - V_R}{V_{NR}} \cdot 100[\%] \tag{7}$$

$$\varepsilon_T = \frac{T_{NR} - T_R}{T_{NR}} \cdot 100[\%] \tag{8}$$

The results of the parameter α_δ and of the discrepancies ε_V and ε_T, which represent indicators of the floor in-plane behaviour, were analysed to study the influence of five variable parameters used in the parametric analyses, namely the dimensionless distance between the central longitudinal wall and the outer walls *i/L*, the number of storey *N*, the stiffness per unit length of the floor panel-to-panel connection $K_{f\text{-}f}$, the stiffness per unit length of the floor-to-wall connection $K_{f\text{-}w}$, and the shear-wall stiffness configuration (*S1*, *S3* or *S5*).

Moreover, the values of the parameter α_δ and the discrepancies ε_V and ε_T were analysed in relation to the ratio κ between the in-plane stiffness of the floor, K_{floor}, and the average stiffness of the shear-walls of the SFRS, K_{wall}, see Eq. (9). This ratio describes the in-plane behaviour of the floor within the structural system, being proportional to the relative in-plane deformation of the CLT floor diaphragm and the CLT shear-walls.

For the calculation of the ratio κ, the in-plane stiffness of the floor and the average stiffness of the shear-walls, a subsystem within the CLT platform archetype considered in the parametric analysis was considered, see Fig. 10a. The subsystem considered includes the portion of floor between two adjacent shear-walls, along with the two shear-walls themselves, thus enabling a local evaluation of the in-plane behaviour of the floor. It should be noted that the deformation mechanism of the subsystem considered for the calculation of the ratio κ, (Fig. 10a), differs from the actual deformation mechanism of the CLT archetype, as qualitatively shown in Fig. 10b. This simplifying assumption on the deformation mechanism was made to simplify the analytical calculation of the floor stiffness in the floor region between two consecutive shear-walls, enabling the methodology to be generalized and applied to CLT buildings with various geometries and plan shapes.

$$\kappa = \frac{K_{floor}}{K_{wall}} \tag{9}$$

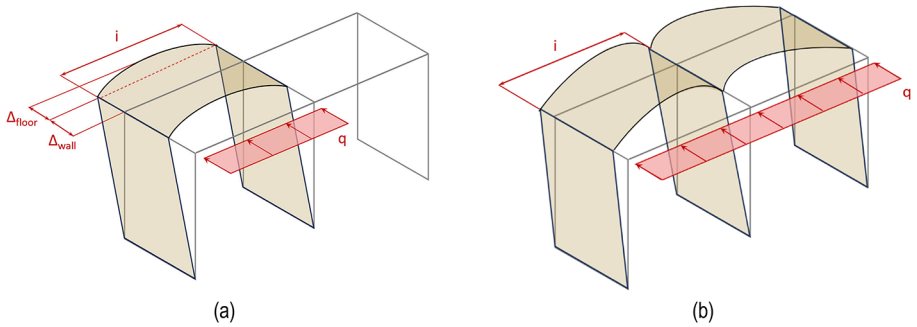

Fig. 10 **a** Deformation mechanism assumed for the subsystem considered for the calculation of the ratio κ; **b** qualitative actual deformation mechanism of the CLT archetype

In this subsystem, the in-plane stiffness of the floor can be calculated with Eq. (10), proposed in the current study, where t_f is the thickness of the CLT floor panels and $G_{eff,floor}$ represents the effective shear modulus of the CLT floor panels. Equation (10) assumes an elastic behaviour of the floor and considers only the shear deformation mechanism of the floor, while neglecting the bending deformation mechanism (see D'Arenzo et al. (2019)). In particular, it considers the displacement contribution of the panel-to-panel connections and the panel shear deformation, while neglecting the displacement contribution of the floor-to-wall connections and the panel bending deformation, see Fig. 11a. The correctness of Eq. (10) was verified by means of FE simulations of CLT floors with different geometries and mechanical properties.

$$K_{floor} = \frac{q \cdot i}{\Delta_{floor}} = \left(\frac{\frac{i}{b} + \frac{b}{i} - 2}{8 \cdot K_{f-f} \cdot L} + \frac{i}{8 \cdot G_{eff,floor} \cdot t_f \cdot L} \right)^{-1} \tag{10}$$

On the other hand, the lateral stiffness of a single shear-wall can be calculated with Eq. (11), according to Casagrande et al. (2016) and Seim et al. (2014), by considering the sliding and rocking deformation mechanism of the wall and the shear panel deformation, while neglecting the panel bending deformation contribution, see Fig. 11b. Equation (11) assumes an elastic behaviour of the wall and can be used for both the external and the inner walls, being independent on the wall position.

$$K_{wall} = \frac{q \cdot i}{2 \cdot \Delta_{wall}} = \left(\frac{1}{K_{AB}} + \frac{h^2}{\sum_{i=1}^{n} K_{V,i} x_i^2} + \frac{h}{G_{eff,wall} \cdot t_w \cdot l} \right)^{-1} \tag{11}$$

In Eq. (11), K_{AB} is the horizontal stiffness of all angle brackets, $K_{V,i}$ is the vertical stiffness of the ith connector on the wall base, x_i is the distance of the ith connector from the centre of rotation of the wall, assumed in this model 10% of the wall length according to Casagrande et al. (2016) and Seim (2024) to take into account the deformability of the timber in the compression zone, t_w is the thickness of the CLT wall panel, and $G_{eff,wall}$ represents the effective shear modulus of the wall panel.

It should be noted that the condition for rigid floor diaphragms, given in Eq. (6), can be expressed as a function of the stiffness of the wall and the stiffness of the floor, allowing for the derivation of an upper bound limit for the ratio κ to ensure a rigid in-plane behaviour of

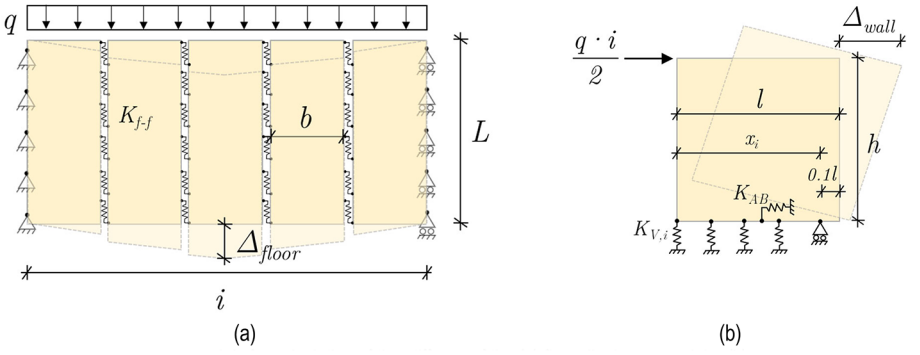

Fig. 11 Analytical models for calculation of the stiffness of the **a** floor diaphragm and the **b** shear-wall

the floor. Considering the deformation mechanism depicted in Fig. 10a, Eq. (6) can be written as function of the ratio between the displacement of the floor, Δ_{floor}, and the displacement of the wall, Δ_{wall}, as presented in Eq. (12). By considering that the displacement of the floor and the displacement of the wall can be written as function of their respective stiffness, as shown in Eq. (13), the condition for rigid floor diaphragms can be further expressed as function of the ratio κ between the stiffness of the floor and the stiffness of the wall, as presented in Eq. (14).

$$\Delta_{floor} + \Delta_{wall} = (1 + \alpha_\delta)\Delta_{wall} \rightarrow \frac{\Delta_{floor}}{\Delta_{wall}} = \alpha_\delta \tag{12}$$

$$\Delta_{floor} = \frac{q \cdot i}{K_{floor}} \text{ (a) } \Delta_{wall} = \frac{q \cdot i}{2 \cdot K_{wall}} \text{(b)} \tag{13}$$

$$\kappa = \frac{K_{floor}}{K_{wall}} = \frac{2}{\alpha_\delta} \tag{14}$$

4 Parametric analysis: results

This section presents the results of the parametric analysis on the CLT platform archetype. By way of example, Fig. 12 shows the deformed configuration of the CLT platform archetype in the case of shear-wall stiffness *S1*, floor panel-to-panel connection stiffness of $K_{f\text{-}f}$=2 N/mm, floor-to-wall connection stiffness of $K_{f\text{-}w}$=3 N/mm, archetype transversal dimension of B=10 m, and archetype longitudinal dimension of L=5 m.

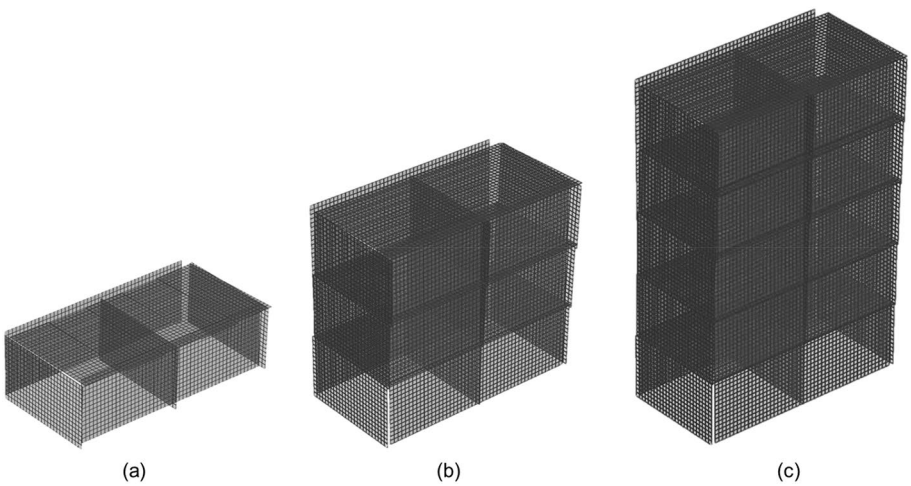

Fig. 12 Deformed configuration of the numerical model of the CLT platform archetype: **a** single-storey, **b** three-storey, **c** five-storey

4.1 The influence of the variable parameters

The values of the parameter α_δ related to the maximum lateral horizontal displacement of the CLT floor diaphragm are plotted in Fig. 13 and Fig. 14 as function of the dimensionless distance between the central shear-wall and each of the two outer longitudinal shear-walls *i/L*, for a value of stiffness of the floor-to-wall connection per unit length $K_{f\text{-}w}$ equal to 3 and 45 N/mm^2, respectively. The results are organized in a matrix form. Each cell in the matrix presents the results for the three selected values of the stiffness per unit length of the floor panel-to-panel connections ($K_{f\text{-}f}$) and the three different configurations of archetypes in terms of shear-wall stiffness (*S1*, *S3* and *S5*). Within each cell of the matrix, five curves are reported. These curves correspond to the five selected numbers of storeys (one to five). Each point of the curves refers to the storey where the greatest value of α_δ is obtained.

An increasing trend of α_δ is observed for increasing values of the parameter *i/L*, while α_δ decreases when the stiffness of the floor panel-to-panel connections ($K_{f\text{-}f}$) increases. More interestingly, it can be noted that α_δ decreases for increasing values of the number of storeys, *N*, and it increases as the stiffness of the floor-to-wall connections ($K_{f\text{-}w}$) increases. Figure 13 (referring to $K_{f\text{-}w}$=3 N/mm^2) shows that α_δ is always lower than 10% for $K_{f\text{-}f}$=20 N/mm^2 and number of storeys $N>2$, for any values of shear-wall stiffness (*S1* to *S5*) and dimensionless distance *i/L* considered in the parametric analysis. On the other hand, for $K_{f\text{-}f}$=8 N/mm^2, α_δ is lower than 10% only for values of the parameter $i/L<1.4$ and number of storeys $N>2$. For higher floor-to-wall connection stiffnesses (see Fig. 14 referring to $K_{f\text{-}w}$=45 N/mm^2), the parameter *i/L* play a more import role, with the maximum values of the parameter α_δ increasing for increasing values of the dimensionless distance *i/L*. In this case, values of the parameter α_δ lower than 10% are found for $K_{f\text{-}f}$=20 N/mm^2, number of

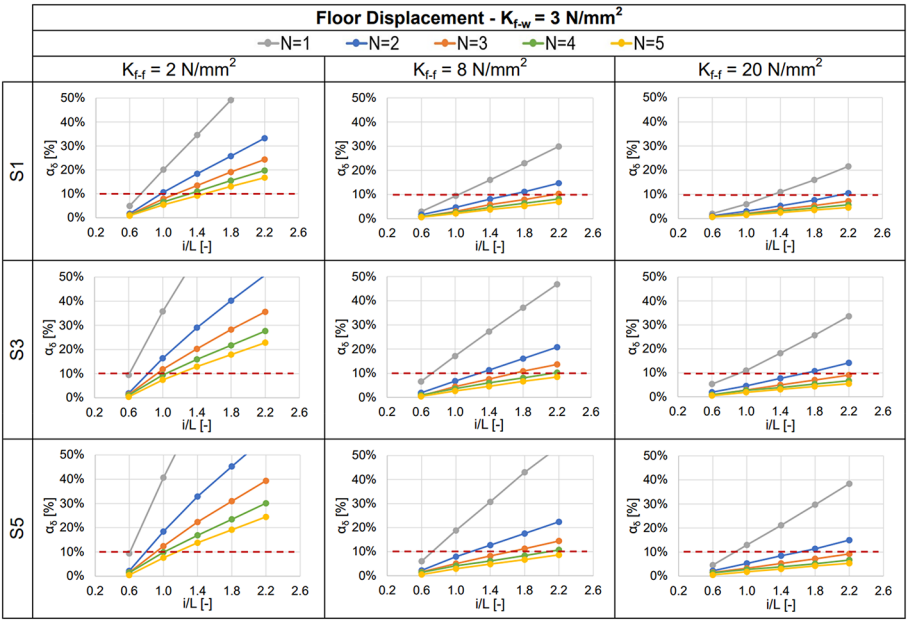

Fig. 13 Maximum values of the parameter α_δ, plotted against the ratio i/L, in case of $K_{f\text{-}w}$=3 N/mm.^{2}

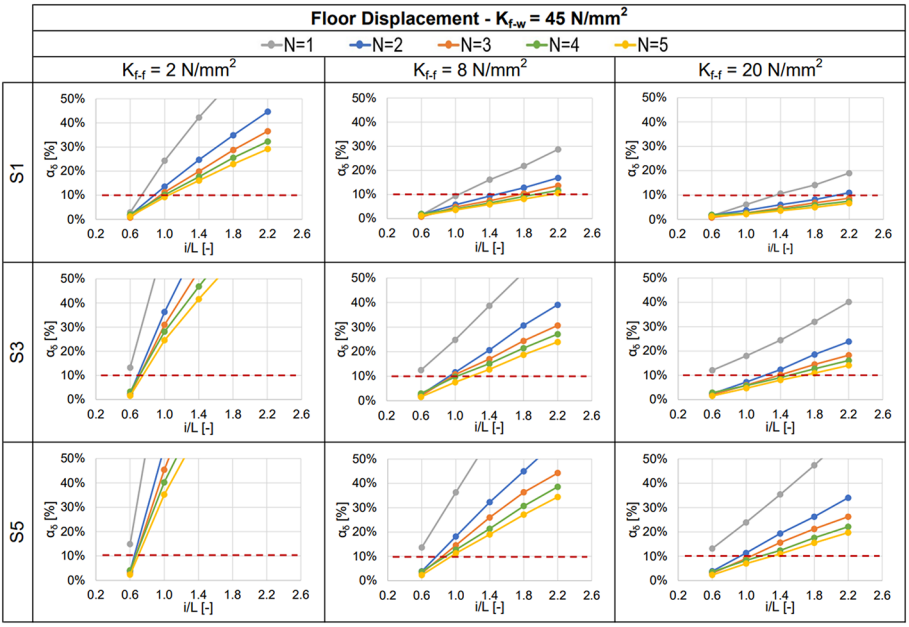

Fig. 14 Maximum values of the parameter α_δ, plotted against the ratio i/L, in case of $K_{f\text{-}w}$=45 N/mm.[2]

storeys $N>1$, dimensionless distance $i/L<1.0$, for any values of shear-wall stiffness (*S1* to *S5*) considered in the parametric analysis.

The maximum values of discrepancy ε_V related to the shear force acting on the central shear-wall is shown in Fig. 15 as function of the dimensionless distance *i/L*, for a value of the stiffness of floor-to-wall connections per unit length $K_{f\text{-}w}$=45 N/mm^2. The curves show trends similar to those reported in Fig. 13 and Fig. 14, but generally lower values of ε_V than those found for α_δ are found since all values of ε_V are in the range between 0 and 25%. In general, values of ε_V lower than 10% are obtained for stiffness of the floor panel-to-panel connection $K_{f\text{-}f}$=20 N/mm^2, number of storeys $N>1$, $K_{f\text{-}w}\leq$45 N/mm^2, dimensionless distance $i/L\leq1.4$, for any values of shear-wall stiffness (*S1* to *S5*) considered in the parametric analysis. As shown in Fig. 16, the values of ε_V obtained for $K_{f\text{-}w}$=45 N/mm^2 are always greater than those obtained for values of $K_{f\text{-}w}$=3 kN/mm^2 and $K_{f\text{-}w}$=15 kN/mm^2, representing hence the most stringent condition.

The values of discrepancies ε_T related to the fundamental period *T* are plotted in Fig. 17 as function of the dimensionless distance *i/L*. The trends of the curves are similar to those shown for α_δ and ε_V. For values of floor panel-to-panel connection stiffness $K_{f\text{-}f}$=2 N/mm^2, ε_T is not greater than 50%, whereas, for $K_{f\text{-}f}$=20 N/mm^2, ε_T is not greater than 20%. Values of ε_T lower than 10% are obtained for $K_{f\text{-}f}$=20 N/mm^2, number of storeys $N>1$, $K_{f\text{-}w}\leq$45 N/mm^2, for any values of shear-wall stiffness (*S1* to *S5*) and dimensionless distance *i/L* considered in the parametric analysis. Similarly to the results obtained for ε_V, as shown in Fig. 18, the values of ε_T obtained for $K_{f\text{-}w}$=45 N/mm^2 are always greater than those obtained for values of $K_{f\text{-}w}$=3 N/mm^2 and $K_{f\text{-}w}$=15 N/mm^2, representing hence the most stringent condition.

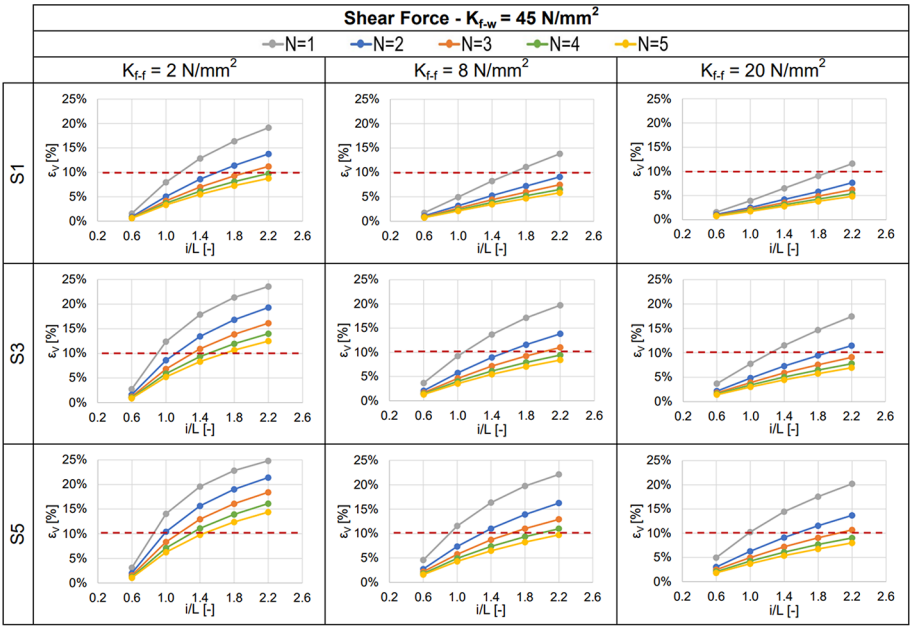

Fig. 15 Maximum discrepancy ε_V plotted against the ratio i/L, in case of $K_{f\text{-}w}$=45 N/mm.^{2}

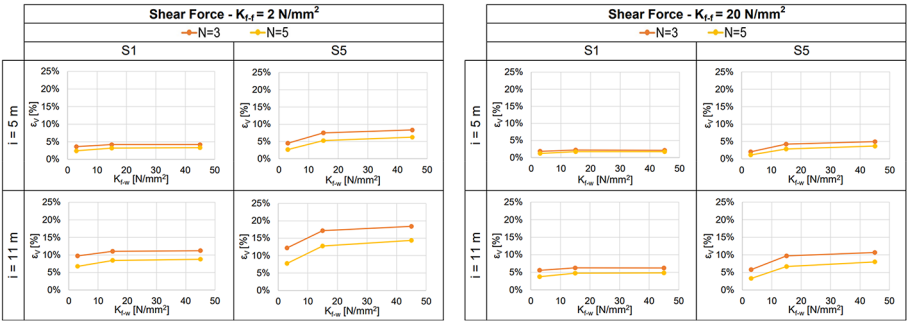

Fig. 16 Maximum discrepancy ε_V plotted against the floor-to-wall connection stiffness, $K_{f\text{-}w}$

4.2 The influence of the ratio between the floor stiffness and the shear-wall stiffness

The values of the parameter α_δ and the discrepancies ε_V and ε_T were also analysed by considering the influence of the ratio κ between the in-plane stiffness of the floor K_{floor} and the average stiffness of the shear-wall K_{wall}, as previously described in Sect. 3.3. In particular, for the calculation of κ, the stiffness K_{floor} was calculated considering the portion of floor between two consecutive shear-walls, whereas the K_{wall} was calculated considering the average stiffness of the two consecutive shear-walls (see Fig. 10a).

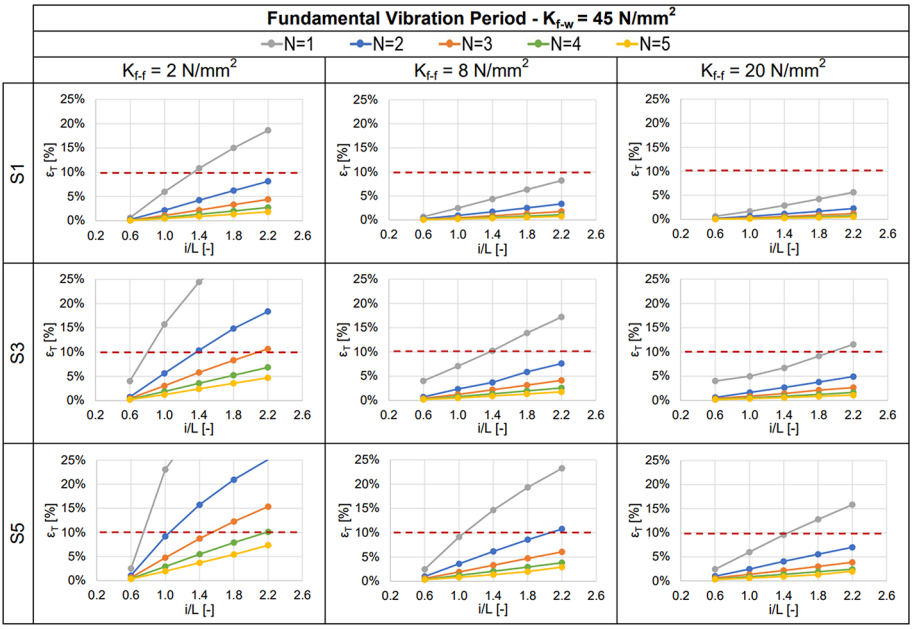

Fig. 17 Maximum discrepancy ε_T plotted against the ratio i/L, in case of $K_{f\text{-}w}$=45 N/mm.^{2}

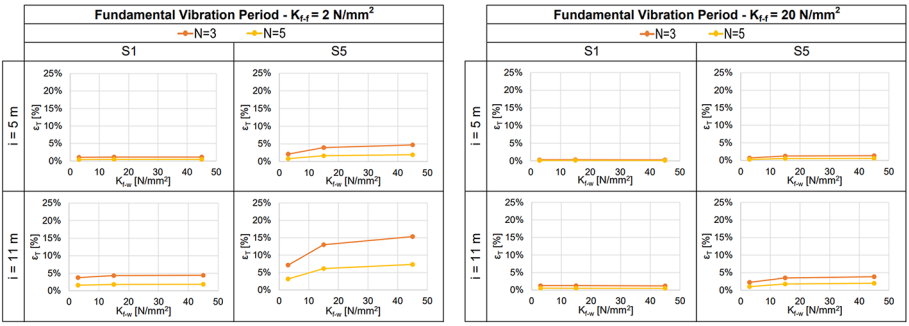

Fig. 18 Maximum discrepancy ε_T plotted against the floor-to-wall connection stiffness, $K_{f\text{-}w}$

The dependency of the parameter α_δ from the ratio κ is plotted in a logarithmic scale in Fig. 19 in a matrix form as function of the floor-to-wall connection stiffness $K_{f\text{-}w}$ and the number of storeys N, (for $N>1$ the values are related to the floor level where the maximum values of α_δ were obtained). As expected, a decreasing trend of the parameter α_δ is observed with increasing valuers of the ratio κ. A not negligible reduction of α_δ is also observed with the increase of the number of storeys N and with the decrease of the floor-to-wall connection stiffness $K_{f\text{-}w}$. It is noteworthy to observe that for all analysed cases of multi-storey archetypes,α_δ is lower than 0.1 for values of κ larger than or equal to 10.

For each curve of Fig. 19, a power regression equation was determined as expressed by Eq. (15):

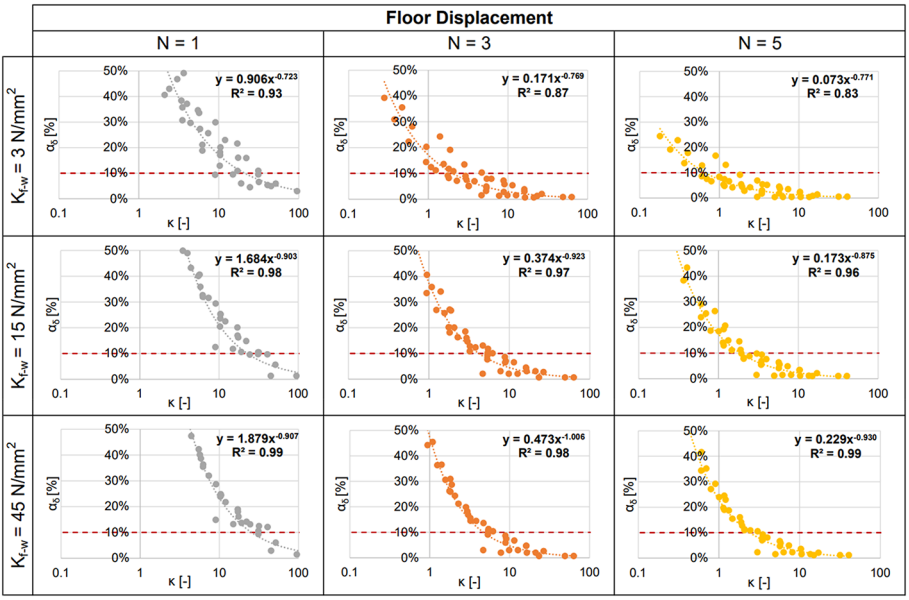

Fig. 19 Maximum value of the parameter α_δ plotted against the ratio κ

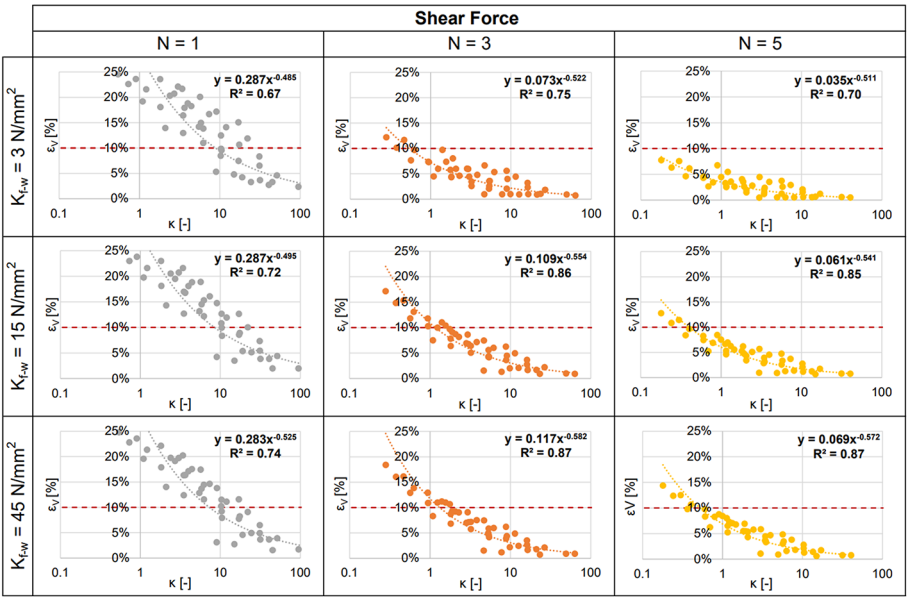

Fig. 20 Maximum discrepancy ε_V plotted against the ratio κ

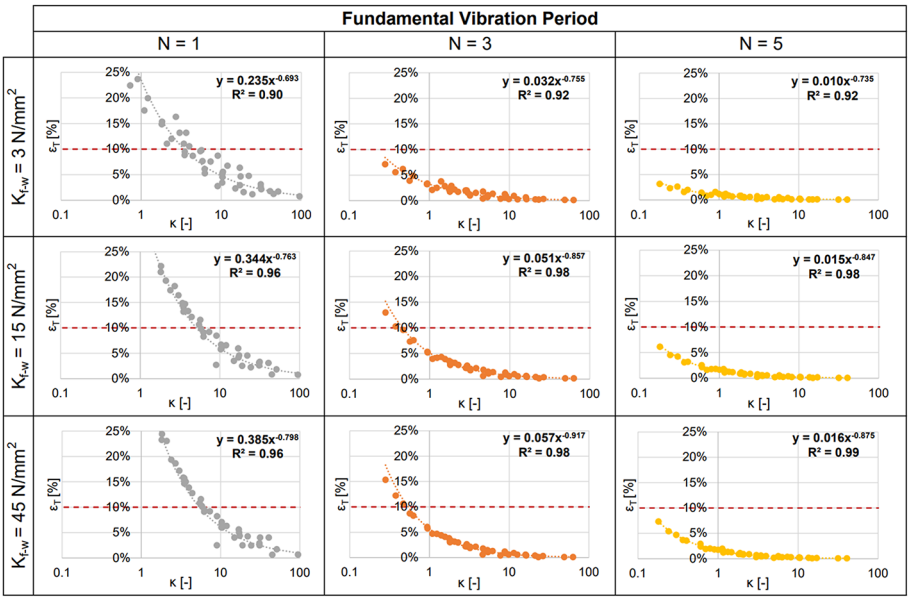

Fig. 21 Maximum discrepancy ε_T plotted against the ratio κ

$$y = a \cdot \kappa^b \tag{15}$$

In Eq. (15), y represents α_δ and a and b are the two parameters governing the power regression equation. The determined values of a and b were in the range of 0.07 to 1.90 and -0.7 and -1.00, respectively. The coefficient of determination R^2 was greater than 0.90 for all cases with $K_{f\text{-}w}$ greater than or equal to 15 N/mm^2 while a R^2 between 0.8 and 0.9 was obtained for values of $K_{f\text{-}w}$ equal to 3 N/mm^2. This difference is reasonably related to the assumptions used for the definition of the in-plane stiffness of the floor, in which only the shear deformation mechanism was considered. In fact, when low values of $K_{f\text{-}w}$, the bending deformation of the floor may contribute to the global flexibility of the floor according to D'Arenzo et al. (2019).

In Fig. 20 and Fig. 21 the dependency of the discrepancy ε_V and ε_T from the ratio κ is plotted in a logarithmic scale in the same matrix form used for the parameter α_δ.

The results for ε_V shows a slighter decreasing trend than that observed for parameter α_δ with also a smaller influence of both $K_{f\text{-}w}$ and the number of storey N. The values of the coefficient of determination R^2 are approximately in the range of 0.65 and 0.80, showing an overall larger dispersion of the obtained values. Also in this case, for each curve a power regression equation was determined as expressed by Eq. (15), where in this case y represents ε_V and the values of a and b are in the range of 0.03 to 0.30 and -0.45 to -0.60, respectively. In this case, in case of multi-storey archetypes, ε_V is always lower than 10% for values of κ larger than 4.

Table 4 Conditions of rigid floor diaphragm for single-storey and multi-storey CLT archetypes as a function of the variable parameters

	N = 1			N > 1		
	$K_{f\text{-}f}$	$K_{f\text{-}w}$	i/L	$K_{f\text{-}f}$	$K_{f\text{-}w}$	i/L
	[N/mm^2]	[N/mm^2]	[−]	[N/mm^2]	[N/mm^2]	[−]
$\varepsilon_V \leq 10\%$	≥20	≤45	≤1.0	≥20	≤45	≤1.4
$\varepsilon_T \leq 10\%$	≥20	≤45	<1.4	≥20	≤45	≤2.2
$\alpha_\delta \leq 10\%$	≥20	≤45	<0.6	≥20	≤45	≤1.0
					≤3	≤1.4

Table 5 Conditions of rigid floor diaphragm for single-storey and multi-storey CLT archetypes as a function of κ

	N = 1	N > 1
	κ	κ
	[−]	[−]
$\varepsilon_V \leq 10\%$	≥15	≥4
$\varepsilon_T \leq 10\%$	≥5	≥1
$\alpha_\delta \leq 10\%$	≥25	≥10

The observations for ε_T are not much different from those obtained for ε_V with the only exception that a much smaller dispersion of the values of data was obtained. The values of the coefficient of determination R^2 are approximately in the range of 0.90 and 1.00. The power regression equation was determined as expressed by Eq. (15), where in this case y represents ε_T and the values of a and b are in the range of 0.01 to 0.40 and -0.65 and -0.95, respectively. In this case, in case of multi-storey archetypes, ε_T is always lower than 10% for values of κ larger than 1.

5 Rigid floor diaphragm conditions for the analysed archetypes

The results reported in the previous section are adopted to define the conditions for which CLT floors of the analysed archetypes can be assumed to be modelled as rigid for linear seismic analyses.

Imposing an upper limit value of the floor displacement parameter α_δ not greater than 10% according to Eurocode 8 (EN1998-1) and, accepting a maximum value for the discrepancy related to the shear forces on the inner shear-walls ε_V and of the discrepancy on the natural period of the archetype ε_T not greater than 10%, the conditions of rigid floor diaphragm are summarized in Table 4 for single-storey and multi-storey archetypes.

The analyses conducted considering the ratio κ between the floor stiffness K_{floor} and the shear-wall stiffness K_{wall} also reveal that both the floor displacement parameter α_δ and the value of discrepancy ε_V and ε_T are not greater than 10% for the values of ratio κ presented in Table 5. It should be noted that the limit values of κ that ensures $\alpha_\delta \leq 0.1$ for one-storey archetype is consistent with the values of κ that would be obtained from Eq. (14) for a value of α_δ equal to 0.1 ($\kappa = \frac{2}{\alpha_\delta} = \frac{2}{0.1} = 20$). The difference between the values of 25 and 20 may be due to several aspects, such as the fact that the CLT archetype consists of three shear-walls rather than two or the fact that in the calculation of κ, the floor stiffness is calculated with an analytical model that considers only the shear deformation of the floor.

However, in case of multi-storey archetypes, the limit value of κ is equal to 10. This discrepancy from the condition obtained for one-storey archetype is primarily due to a more complex interaction that exists between floors and shearwalls in multi-storey lateral load resisting systems.

A preliminary validation of the proposed conditions is presented in Appendix A, where two case studies representing real cases of CLT platform-type buildings are considered. These cases provide initial insights into the applicability of the conditions derived from the parametric analysis.

6 Conclusions

This paper presented a numerical study on the in-plane stiffness of CLT floor diaphragms in CLT platform-type buildings. The study investigated the in-plane behaviour of CLT floor diaphragms, in the context of linear seismic analyses, considering the provisions of different international design codes and in particular Eurocode 8 (EN1998-1).

The study was addressed by considering numerical analyses of a CLT platform archetype with regular geometry. Within a parametric analysis framework, the most influential geometrical and mechanical properties of the structure, such as the ratio between the distance between two consecutive shear-walls and the floor span i/L, the stiffness of the floor panel-to-panel connections $K_{f\text{-}f}$, the stiffness of the floor-to-wall connections $K_{f\text{-}w}$, the lateral stiffness of the shear-walls K_{wall}, and the number of storeys N, were varied, to define the geometrical and mechanical conditions for which the assumption of rigid floor diaphragm may be adopted in linear seismic analysis with reasonable accuracy.

The stiffness properties of the connections of the floor were selected based on a state-of-the-art review presented in the paper, differentiating between low, medium, and high stiffness values, whereas the other geometrical and mechanical properties of the structures were chosen to be representative of construction practices.

Furthermore, the study focused on evaluating the in-plane behaviour of CLT floors by considering the ratio κ between the in-plane stiffness of the floor K_{floor} and the shear-wall lateral stiffness K_{wall}. A simplified analytical model is proposed to calculate the in-plane stiffness of the floor, whereas a model from the literature in considered for the calculation of the shear-wall lateral stiffness.

The evaluation of the in-plane behaviour of the floors was conducted by comparing the results in terms of floor displacements, distribution of the shear force in the shear-walls, and the natural period of the structure, of numerical models where the in-plane behaviour of the floor was considered with its actual deformability and as rigid. The discrepancies of the results of the models with actual deformability and rigid behaviour of the floor were compared with threshold values reported in Eurocode 8 (EN1998-1) and were used to evaluate the floor in-plane behaviour.

With this approach, the rigid floor diaphragm conditions were derived.

Based on the analyses conducted in this study, the following conclusions can be drawn:

- The in-plane behaviour of the floor tends toward the rigid diaphragm condition by increasing the stiffness of the floor panel-to-panel connections $K_{f\text{-}f}$ and the number of storeys N, and by decreasing the stiffness of the floor-to-wall connections $K_{f\text{-}w}$, the ratio

between the distance between two consecutive shear-walls and the floor span i/L, and the stiffness of the shear-walls K_{wall}.

- An in-plane rigid behaviour with discrepancies in terms of floor displacements, shear force distributions and fundamental period lower than 10% was observed for floor panel-to-panel connection stiffnesses $K_{f\text{-}f} \geq 20$ N/mm^2, floor-to-wall connection stiffnesses $K_{f\text{-}w} \leq 45$ N/mm^2, ratio between the distance of two consecutive shear-walls and the span of the floor $i/L \leq 1.0$, and number of storeys $N > 1$. More rigid diaphragm conditions can be found in Table 4.
- The ratio κ between the stiffness of the floor, K_{floor}, and the shear-wall stiffness, K_{wall}, is a good indicator of the in-plane behaviour of the floor. The results of the parametric analysis of the multi-storey archetypes showed an in-plane rigid behaviour with discrepancies in terms of floor displacements, shear force distribution and fundamental period always lower than 10% for values of $\kappa = \frac{K_{floor}}{K_{wall}} \geq 10$, providing an easy-to-use condition to evaluate the in-plane behaviour of CLT floors in CLT platform-type structures.

The conditions outlined above where derived based on analysis of a reference CLT building with regular geometry, representing ideal conditions rather that real cases. Therefore, validation of the proposed methodology on CLT platform-type structures with real case studies is necessary to ensure its reliability and applicability in practical scenarios.

As a first attempt to validate the methodology, two CLT buildings representing real cases were considered (Appendix A). These initial comparisons revealed discrepancies in terms of floor displacements, distribution of shear force in the shear-walls, and the natural period of the structure, which were close to those obtained in the analysis of the reference CLT building.

The findings of the current study may have significant implications for current design standards, such as Eurocode 8. The results of the study suggest potential updates to the provisions related to the in-plane stiffness requirements for CLT floor diaphragms, particularly in the context of linear seismic analyses. The conditions derived for achieving a rigid diaphragm behaviour may serve as guidelines for refining the criteria in Eurocode 8, ensuring more accurate and reliable seismic performance predictions for CLT platform-type structures.

Appendix

A: Case studies

In this section, two case studies are presented to provide a preliminary validation of the rigid diaphragm conditions discussed in Sect. 5, which were derived from the parametric analysis conducted on the CLT archetypes described in Sect. 3.1. These case studies aim to highlight potential differences and assess the applicability of the proposed conditions to real-world scenarios.

A.1. Description of the case studies and method of analysis

The first case study consists of a two-storey CLT building with plan dimensions of 7.80 × 8.00 m. 5-ply 100 mm and 5-ply 158 mm CLT panels are used as for shear-walls and floor elements at both storeys. The shear-walls are anchored to the foundation and to the storey below by means of either one or two WHT440 hold-downs connected to the CLT panels with thirty 4 × 60 mm annular ring nails and by AE116 angle brackets connected to the panels with 25 annular ring nails 4 × 60 mm. The layout of shear-walls and floor elements as well as the layout and the number of hold-downs and angle-brackets adopted per each shear-wall is shown in Fig. 22. The panel-to-panel connections of the floor elements were made with spline joints, where 8 × 140 mm PTSs with a spacing of 300 mm were used, whereas PTSs 10 × 320 mm with spacing of 230 mm were used for the floor-to-wall connections.

A five-storey CLT buildings with plan dimensions of 20.00 × 7.00 m is analysed as second case study. CLT wall panels of different thickness along the building height are used, namely: 5-ply 140 mm at the first floor, 5-ply 120 mm at the second and third floor, and 5-ply 100 mm at the two upper storeys. 5-ply 140 mm CLT panels were used as floor elements at all storeys. The shear-walls are anchored to the foundation and to the storey below by means of either WHT740 hold-downs and WHT620 hold-downs connected with seventy-five and fifty-five 4 × 60 mm annular ring nails, respectively, and TCN240 angle brackets fastened with 30 annular ring nails 4 × 60 mm. The layout of the shear-walls and floor elements as well as of the number and layout of mechanical anchors (Hold-down and angle brackets) are shown in Fig. 23. The panel-to-panel connections of the floors were made with a combination of butt joint with inclined 7 × 180 mm FTS with spacing of 300 mm, whereas two 45° FTSs 11 × 400 mm with spacing of 350 mm were used for the floor-to-wall connections.

The analyses were conducted with the same strategy as that adopted for the CLT archetypes described in Sect. 3. The uniform distributed loads calculated through a linear static analysis were applied at the floors of each storey parallel to the floor panels. A peak ground acceleration equal to 0.22 g with a soil type C according to the Italian National Building Code (D.M.17/01/2018.) was adopted for the seismic design of both buildings.

For each case study, the analyses were carried out both first on a finite element model (developed according to the procedure described in Sect. 3.2) of the building where the actual deformation (i.e. non-rigid floor model) of the floor diaphragm was considered, and

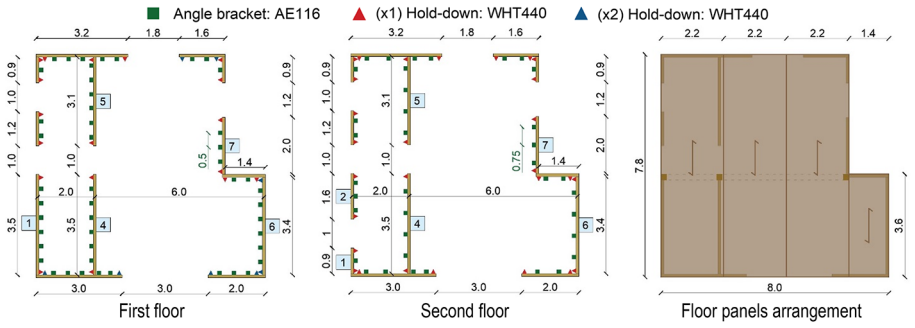

Fig. 22 First case study used for the validation

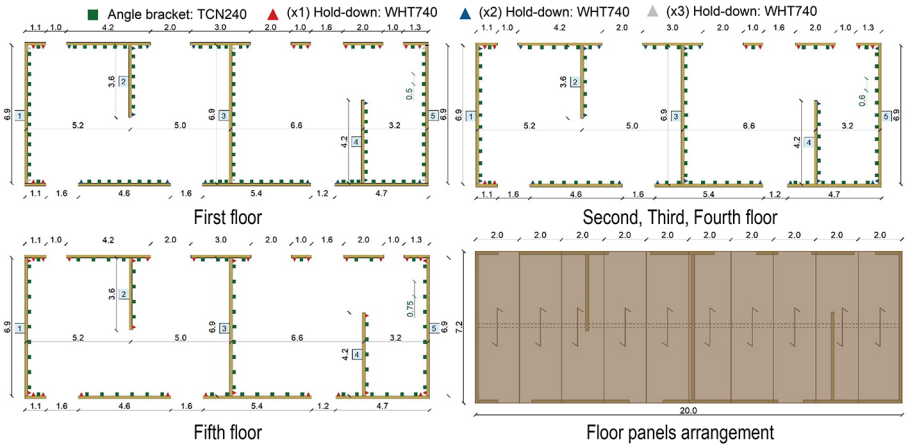

Fig. 23 Second case study used for the validation

then on the model where rigid diaphragm constraints were applied simulating the rigid diaphragm condition.

The comparison between the non-rigid floor and rigid floor models was conducted calculating the parameters α_δ, representing the increase of displacement when the floor is modelled with its actual deformation, as well as the discrepancies ε_V and ε_T, representing the differences of the total shear forces in the shear-walls and the building natural periods, respectively, between the model where the floor was modelled with its actual deformation and the model with rigid floor.

A.2. Results and discussion: calculation of the values of $\alpha_\delta, \varepsilon_V, \varepsilon_T$

The parameters α_δ are obtained from the two case studies on each floor as reported in Table 6. In both cases, the maximum values are reached at the first floor consistently with the results obtained for the archetypes and are not greater than 3.5%.

The absolute values of discrepancies ε_V are reported in Table 7 for both case studies for all shear-walls parallel to the load direction with a length greater than 1.2 m. The obtained

Table 6 Storey displacements and α_δ values of the two case studies

Storey	Non-rigid	Rigid	α_δ
[−]	[mm]	[mm]	[%]
Case study 1			
1st	4.5	4.4	2.71
2nd	9.2	9.0	1.61
Case study 2			
1st	26.9	26.1	3.27
2nd	68.7	66.7	3.02
3rd	122.2	119.3	2.46
4th	176.4	173.1	1.95
5th	225.2	223.1	0.94

Table 7 ε_V values of the two case studies

Wall	ε_V[%]					
ID	l [m]	1st storey	2nd storey	3rd storey	4th storey	5th storey
Case study 1						
1	3.5	1.9	1.9			
4	3.5	0.5	0.6			
6	3.4	0.8	1.6			
5	3.1	0.5	0.7			
7	2	7.4	3.8			
Case study 2						
1	6.9	3.3	3.5	2.5	1.1	6.5
3	6.9	5.8	4.8	4.1	2.3	9.0
5	6.6	4.5	4.6	3.7	1.9	6.1
4	4.2	0.5	2.1	0.9	0.1	7.3
2	3.6	3.5	7.0	5.6	2.8	26.3

Table 8 ε_T values of the two case studies

Non-rigid	Rigid	ε_T
Case study 1		
[sec]	[sec]	[%]
0.274	0.269	1.78
Case study 2		
0.695	0.687	1.21

values are not greater than 10% with the only exception of wall #2 located at the 5th storey of case study 2, for which a discrepancy equal to 26% was obtained. It is noteworthy to mention that this wall was loaded with the lowest shear load compared to all the other shear-walls on the same floor, representing only 1% of the total floor shear load.

The discrepancies ε_T are reported in Table 8 showing values lower than 2% in both case studies.

From the low values of the parameters α_δ and the discrepancies ε_V and ε_T obtained from the analyses, it seems reasonable to assume that the rigid diaphragm conditions are acceptable for both case studies. Adopting a rigid constraint at floor levels did not cause a significant variation in terms of floor displacement, shear loads in the shear-walls and natural period of the building.

A.3. Results and discussion: validation of rigid diaphragm conditions

To validate the results of the parametric analysis with the CLT archetypes and their applicability to real CLT buildings, the results of the two case studies in terms of α_δ, ε_V,ε_T are compared with those obtained from the parametric analysis. The validation was carried out by comparing the values of α_δ, ε_V,ε_T calculated in the two case studies with those obtained in the parametric analysis, considering (i) the variable parameters, namely the dimensionless distance between the central longitudinal wall and the outer walls *i/L*, the number of

storey N, the stiffness per unit length of the floor panel-to-panel connection $K_{f\text{-}f}$, the stiffness per unit length of the floor-to-wall connection $K_{f\text{-}w}$, and the shear-wall stiffness configuration (*S1*, *S3* or *S5*), (results from Figs. 13, 14, 15, 16, 17, 18), and (ii) the ratio κ between the in-plane stiffness of the floor, K_{floor}, and the average stiffness of the shear-walls of the SFRS, K_{wall} (results from Figs. 19, 20, 21).

The variable parameters and the ratio κ of the two case studies are reported in Table 9. As the values of the variable parameters vary depending on the storey considered, the analysis of the variable parameters was focused on the first storeys of the case studies, where the most stringent conditions for a rigid in-plane behaviour of the floors are observed. In this analysis, the values of the stiffness per unit length of the floor panel-to-panel connections, $K_{f\text{-}f}$, and the floor-to-wall connections, $K_{f\text{-}w}$, of the two case studies were calculated using the analytical expressions provided in Eurocode 5 (EN1995-1-1 2008).

For the calculation of the ratio κ, which depends on the floor stiffness K_{floor} and the average shear-wall stiffness K_{wall}, a subsystem as that one shown in Fig. 10 is identified within the considered building, enabling a local evaluation of the in-plane behaviour of the floor. As the ratio κ can be calculated in different regions of the floor between two consecutive shear-walls, the calculation was conducted for all region of the floor between two consecutive shear-walls, and then the maximum value was considered. According to the results of the parametric analyses, the highest values of κ were found in the subsystems with the maximum distance between two consecutive shear-walls at the first storey. The maximum distance between two consecutive shear-walls, i, for case study 1 and case study 2 are equal to 6.0 m and 6.6 m, respectively.

Moreover, in the case of the case study 1, where the floor panels span over multiple shear-walls, an effective shear-wall stiffness $K_{wall,eff}$ was considered for the calculation of κ . The effective shear-wall stiffness $K_{wall,eff}$ was calculated by first summing the stiffnesses of the aligned shear-walls, assuming they work as an in-parallel system, and then taking the average of the two summed stiffnesses, as expressed by:

$$K_{wall,eff} = \frac{K_{set,wall4,5} + K_{set,wall6,7}}{2} = \frac{(K_{wall4} + K_{wall5}) + (K_{wall6} + K_{wall7})}{2} \text{for case study 1}$$

$$K_{\text{wall,eff}} = \frac{K_{wall3} + K_{wall4}}{2} \text{for case study 2}$$

where, the stiffness of each shear-wall was determined according to the analytical procedure expressed in Eq. (11) of Sect. 3.3.

The variable parameters reported in Table 9 were used to predict the values of α_δ, ε_V and ε_T from the parametric analyses conducted with the CLT archetypes. For this, as the variable parameters did not exactly match the values presented in Figs. 13, 14, 15, 16, 17, 18, linear interpolations between the values of the variable parameters were applied. The

Table 9 Geometrical and mechanical properties of the two case studies

Case study	N	$K_{f\text{-}f}$	$K_{f\text{-}w}$	i	L	i/L	$K_{wall,eff}$	K_{floor}	κ
	[−]	[N/mm^2]	[N/mm^2]	[m]	[m]	[-]	[kN/mm]	[kN/mm]	[-]
1	2	9.96	13.83	6.0	7.8	0.77	14.97	334.70	22.36
2	5	9.33	116.51	6.6	7.2	0.91	58.73	218.79	3.73

Table 10 Comparison of α_δ, ε_V, ε_T from the parametric analysis (Figs. 13, 14, 15, 16, 17, 18 and Figs. 19, 20, 21) and the case studies

Case study		Prediction based on i/L, N, $K_{f\text{-}f}$, $K_{f\text{-}w}$, K_{wall} (Figs. 13, 14, 15, 16, 17, 18)			Prediction based on κ (Figs. 19, 20, 21)		
		α_δ [%]	ε_V [%]	ε_T [%]	α_δ [%]	ε_V [%]	ε_T [%]
1	Predicted from archetypes	3.30	2.42	0.73	3.44	2.97	0.87
	Real	2.71	7.40	1.78	2.71	7.40	1.78
2	Predicted from archetypes	6.54	3.51	0.42	9.76	3.87	0.54
	Real	3.27	5.80	1.21	3.27	5.80	1.21

predicted values were then compared with the maximum values obtained from the FE analysis of the case studies (Tables 6, 7, 8).

Table 10 presents the comparison between the values of the variable parameters predicted from the parametric analysis and from the values obtained from the FE analysis of the case studies. It should be noted that, since the value of $K_{f\text{-}w}$ for the case study 2 exceeded the range of the values adopted in the parametric analysis (>45 N/mm^2) the interpolation was conducted by extending the linear trend obtained between the values 15 N/mm^2 and 45 N/mm^2 up to the value of 116.51 N/mm^2.

The results shown in Table 10 indicate relatively close predicted and real values of the parameters α_δ, ε_V and ε_V, confirming that the outcomes derived from parametric analyses conducted with the CLT archetypes can be extended to real cases.

B: Validation of numerical models

This section presents an experimental validation of the numerical modelling strategy of the floor, which was used in the parametric analysis. The experimental tests on CLT floors conducted by Véliz et al. (2024) were used for the validation. A 3.6 × 2.4 m CLT floor in a single-span configuration was considered, as shown in Fig. 24. The floor consisted of three 5-layer CLT panels with a total thickness of 165 mm (each layer measuring 33 mm), a width of 1200 mm, and a length of 2400 mm. The floor panel-to-panel connections were made using outer spline joints and pairs of 5.6 × 150 mm PTSs spaced at 400 mm. The experiment was conducted as a four-point bending test, with two monotonic in-plane loads applied to the central CLT panel and two supports placed at the edges of the two external CLT panels.

The experimental test described above was simulated by using a numerical model developed in SAP2000, following the strategy outlined in Sect. 3.2. The CLT panels were modelled as orthotropic shell elements with a 200 mm mesh size, as illustrated in Fig. 25. The floor panel-to-panel connections were modelled as two-joint links, with linear elastic behaviour assumed in the direction parallel to the joint and bilinear elastic behaviour in the transverse direction to simulate both the separation and contact between panels. The same stiffness value was used in the direction parallel to the joint and in the transverse direction for the separation of the panels. The elastic properties of the CLT panels were calculated using Eq. (1), (2), and (3), with an elastic modulus E_0 equal to 11,600 MPa and a shear modulus

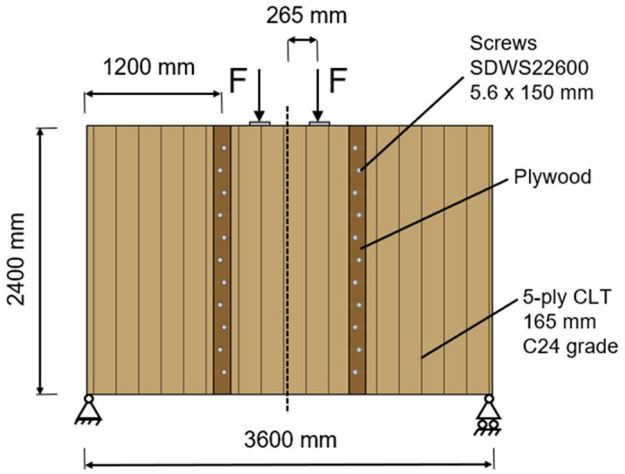

Fig. 24 CLT floor considered for the experimental validation (tests conducted by Véliz et al. (2024))

G_0 equal to 690 MPa for timber. The stiffness of the links simulating the floor panel-to-panel connections was assigned based on the experimental tests conducted by Masroor et al. (2024), where panel-to-panel connections with outer spline joints and 6.0 × 70 mm PTSs were tested. It is important to note that the stiffness value of 1.0 kN/mm found in the tests by Masroor et al. (2024) was scaled by a factor of 0.93 (calculated as the ratio 5.6/6.0) to account for the difference in diameter with the connections used in the experimental tests by Véliz et al. (2024). Consequently, a stiffness of 0.93 kN/mm was considered for the panel-to-panel connections, which, when combined with a spacing of 400 mm, resulted in a stiffness per unit length $K_{f\text{-}f}$ of 2.33 N/mm^2.

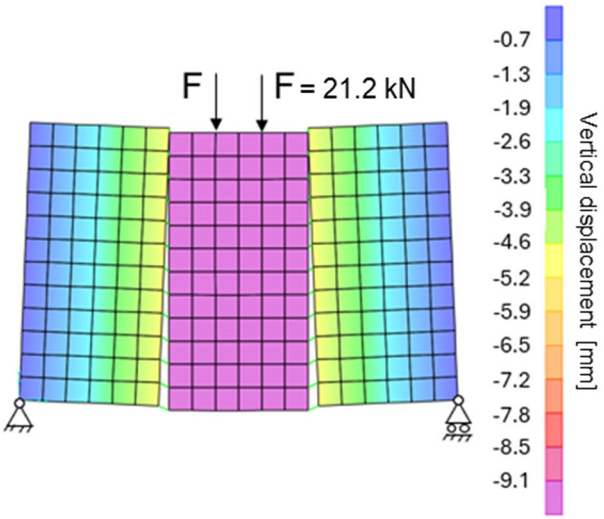

Fig. 25 Deformed configuration of the numerical model of CLT floor considered for the validation

Table 11 Geometric and elastic properties of the floor numerical model

i	L	b	t_{CLT}	n_{lay}	t_{lay}	$K_{f\text{-}f}$	$E_{eff,v}$	$E_{eff,h}$	G_{eff}
[m]	[m]	[m]	[mm]	[-]	[mm]	[N/mm^2]	[N/mm^2]	[N/mm^2]	[N/mm^2]
3.6	2.4	1.2	165	5	33	2.33	6600	4400	490

Table 12 Comparison of the elastic stiffness of the floor numerical model and the experimental tests

$K_{floor,NUM}$	$K_{floor,EXP}$	Discrepancy
[kN/mm]	[kN/mm]	[%]
4.61	4.40	4.88

To simulate the boundary conditions of the experimental tests, two vertical constraints were added to the external corners of the two external CLT panels, and two vertical forces F were applied to the central CLT panel. A non-linear elastic static analysis was performed to account for the non-linearity introduced by the panel-to-panel connections. The geometric and elastic properties of the floor numerical model are provided in Table 11.

Table 12 presents the results in terms of the elastic stiffness of the numerical simulations and the experimental tests. The numerical floor stiffness $K_{floor,NUM}$ was calculated by dividing the total load applied to the floor, i.e.2 F, by the displacement at the floor midspan. The experimental floor stiffness $K_{floor,EXP}$ was determined as the slope of the line passing through the origin and the point on the load–displacement curve of the experimental test with an ordinate equal to 40% of the maximum load. The discrepancy between the numerical and experimental stiffness amounts to 4.88%, demonstrating the reasonable accuracy of the numerical model in predicting the elastic response of CLT floors subjected to in-plane loads.

Acknowoledgments Parts of this publication are based upon work from COST Action CA20139 "Holistic design of taller timber buildings– HELEN", supported by the European Cooperation in Science and Technology (COST). The author Casagrande gratefully thanks the 2024–2026 ReLUIS-DPC Project framework (funded by the Italian Emergency Management Agency, DPC) for the partial financial support given to this study. The same author also acknowledges the Italian Ministry of Universities and Research 378 (MUR), in the framework of the project DICAM-EXC (Departments of Excellence 2023–2027, grant L232/2016). The author D'Arenzo gratefully thanks Prof. Ghasan Doudak for the valuable discussions on the topic of the in-plane behaviour of floors.

Funding Open access funding provided by Aarhus Universitet

References

ASCE (2017) American Society of Civil Engineers. ASCE/SEI 41–17: Seismic Evaluation and Retrofit of Existing Buildings

Ashtari S, Haukaas T, Lam F (2014) In-Plane Stiffness of Cross-Laminated Timber Floors. World Conf Timber Eng 1–10

Barbosa AR, Rodrigues L, Sinha A, et al (2018) Numerical modeling of CLT diaphragms tested on a shake-table experiment. WCTE 2018—World Conf Timber Eng

Beairsto C, Gupta R, Miller TH (2022) Monotonic and cyclic behavior of CLT diaphragms. Pract Period Struct Des Constr 27:1–14. https://doi.org/10.1061/(asce)sc.1943-5576.0000658

Bogensperger T, Moosbrugger T, Silly G (2010) Verification of CLT-plates under loads in plane. 11th World Conf Timber Eng 2010, WCTE 2010 1:231–240

Brandner R, Dietsch P, Dröscher J et al (2017) Cross laminated timber (CLT) diaphragms under shear: test configuration, properties and design. Constr Build Mater 147:312–327. https://doi.org/10.1016/j.conbuildmat.2017.04.153

Brown JR, Li M, Tannert T, Moroder D (2021) Experimental study on orthogonal joints in cross-laminated timber with self-tapping screws installed with mixed angles. Eng Struct 228:111560. https://doi.org/10.1016/j.engstruct.2020.111560

Casagrande D, Doudak G, Vettori M, Fanti R (2021) Proposal for an equivalent frame model for the analysis of multi-storey monolithic CLT shearwalls. Eng Struct 245:112894. https://doi.org/10.1016/j.engstruct.2021.112894

Casagrande D, Rossi S, Sartori T, Tomasi R (2016) Proposal of an analytical procedure and a simplified numerical model for elastic response of single-storey timber shear-walls. Constr Build Mater. https://doi.org/10.1016/j.conbuildmat.2014.12.114

D.M.17/01/2018. Norme Tecniche per le Costruzioni (NTC 2018). Supplemento ordinario alla Gazzetta Ufficiale, n. 42 del 20/02/2018 [in Italian]

D'Arenzo G, Casagrande D, Reynolds T, Fossetti M (2019) In-plane elastic flexibility of cross laminated timber floor diaphragms. Constr Build Mater 209:709–724. https://doi.org/10.1016/j.conbuildmat.2019.03.060

D'Arenzo G, Ruggeri EM, Fossetti M (2024) Lateral performance of cross-laminated timber shear walls connected to perpendicular walls: experimental tests and analytical modeling. J Struct Eng (United States) 150:1–14. https://doi.org/10.1061/JSENDH.STENG-13151

EN1995-1-1 (2008) Eurocode 5: Design of timber structures—Part 1–1: General—Common rules and rules for buildings. European Standard, European Committee for Standardization

EN1998-1 Eurocode 8 (2013) Design of structures for earthquake resistance - Part 1: General rules, seismic actions and rules for buildings

ETA-Denmark (2018) ETA-13/0815. European Technical Assessment European Technical Assessment. Solid wood slab elements to be used as structural elements in buildings. 1–32

ETA-Denmark (2016) ETA-06/0106. European Technical Assessment. dimensional nailing plate (timber-to-timber/timber-to_concrete angle bracket)

ETA-Denmark (2015) ETA-11/0086. European Technical Assessment. Three-dimensional nailing plate (Angle brackets and hold-downs for timber-to-timber or timber-to-concrete or steel connections)

Fakhrzarei M, Daneshvar H, Chui YH (2024) Numerical parametric study of cross-laminated timber diaphragms under in-plane loading. Constr Build Mater 429:136387. https://doi.org/10.1016/j.conbuildmat.2024.136387

Flatscher G (2017) Evaluation and approximation of timber connection properties for displacement-based simulation of CLT wall systems (working title),. Graz University of Technology

Gavric I, Fragiacomo M, Ceccotti A (2015) Cyclic behavior of typical screwed connections for cross-laminated (CLT) structures. Eur J Wood Wood Prod. https://doi.org/10.1007/s00107-014-0877-6

Hossain A, Popovski M, Tannert T (2019) Group effects for shear connections with self-tapping screws in CLT. J Struct Eng 145:04019068. https://doi.org/10.1061/(asce)st.1943-541x.0002357

International Code Council (ICC) (2018) International Building Code (IBC)

Kode A, Amini MO, van de Lindt JW, Line P (2021) Lateral load testing of a full-scale cross-laminated timber diaphragm. Pract Period Struct Des Constr 26:04021001. https://doi.org/10.1061/(asce)sc.1943-5576.0000566

Line P, Nyseth S, Waltz N (2022) Full-scale cross-laminated timber diaphragm evaluation. I: design and full-scale diaphragm testing. J Struct Eng 148:1–13. https://doi.org/10.1061/(asce)st.1943-541x.0003308

Loss C, Frangi A (2017) Experimental investigation on in-plane stiffness and strength of innovative steel-timber hybrid floor diaphragms. Eng Struct 138:229–244. https://doi.org/10.1016/j.engstruct.2017.02.032

Loss C, Hossain A, Tannert T (2018a) Simple cross-laminated timber shear connections with spatially arranged screws. Eng Struct 173:340–356. https://doi.org/10.1016/j.engstruct.2018.07.004
Loss C, Rossi S, Tannert T (2018b) In-plane stiffness of hybrid steel–cross-laminated timber floor diaphragms. J Struct Eng 144:04018128. https://doi.org/10.1061/(asce)st.1943-541x.0002105
Masroor M, Doudak G, Casagrande D (2024) Experimental investigation of dissipative connections in cross-laminated timber shearwalls. Constr Build Mater 413:134828. https://doi.org/10.1016/j.conbuildmat.2023.134828
Moroder D (2016) Floor Diaphragms in multi-storey timber buildings
Moroder D, Smith T, Pampanin S et al (2015) Design of floor diaphragms in multi-storey timber buildings. Journal 23:32
Popovski M, Auclair SC, Chen Z (2023) Performance, analysis, and design of mass timber diaphragms
Popovski M, Gavric I (2016) Performance of a 2-story CLT house subjected to lateral loads. J Struct Eng 142:1–12. https://doi.org/10.1061/(ASCE)ST.1943-541X.0001315
Ruggeri EM, D'Arenzo G, Fossetti M, Seim W (2023) Analysis of different numerical modelling strategies of multi-storey clt shear walls. https://doi.org/10.52202/069179-0323
Seim W (2024) Structural Timber Design. Ernst & Sohn GmbH, Berlin
Seim W, Hummel J, Vogt T (2014) Earthquake design of timber structures—remarks on force-based design procedures for different wall systems. Eng Struct 76:124–137. https://doi.org/10.1016/j.engstruct.2014.06.037
Véliz F, Chacón MF, Lagos J et al (2024) Structural performance of strong timber diaphragms: high-capacity light-timber frames and cross-laminated timber. Structures. https://doi.org/10.1016/j.istruc.2024.106335
Xiong HB, Huynh A (2018) Mechanical behaviour of connections between CLT panels under monotonic and cyclic loading. IOP Conf Ser Earth Environ Sci. https://doi.org/10.1088/1755-1315/153/4/042014
Yin T, Zhang J, Wang Z et al (2022) Shear performance of tongue-and-groove joints for CLT. Constr Build Mater. https://doi.org/10.1016/j.conbuildmat.2022.126449

Authors and Affiliations

Giuseppe D'Arenzo[1] · Pietro Rigo[2,3] · Valentino Nicolussi[2,3] · Luca Pozza[2] · Daniele Casagrande[4]

✉ Giuseppe D'Arenzo
giuseppe.darenzo@cae.au.dk

[1] Department of Civil and Architectural Engineering, Aarhus University, Inge Lehmanns Gade, 10, 8000 Aarhus C, Denmark

[2] Department of Civil, Chemical, Environmental and Materials Engineering, University of Bologna, Bologna, Italy

[3] Institute of Bioeconomy, National Research Council of Italy, Via Francesco Biasi, 75, 38098 San Michele all'Adige, Trento, Italy

[4] Department of Civil, Environmental and Mechanical Engineering, University of Trento, Via Mesiano 77, 38123 Trento, Italy